Lithos 402–403 (2021) 105756

Contents lists available at ScienceDirect

Lithos

journal homepage: www.elsevier.com/locate/lithos

Research Article

Formation of tin ore deposits: A reassessment

Bernd Lehmann *

Technische Universität Clausthal, Mineral Resources, Adolph-Roemer-Strasse 2A, 38678 Clausthal-Zellerfeld, Germany

ARTICLE INFO

Article history:
Received 30 April 2020
Received in revised form 8 August 2020
Accepted 24 August 2020
Available online 28 August 2020

Keywords:
Tin
Metallogeny
Ore deposits
Geochemistry

ABSTRACT

About 85% of all historically mined tin of about 27 million tonnes Sn is from a few tin ore provinces within larger granite belts. These are, in decreasing importance, Southeast Asia (Indonesia, Malaysia, Thailand, Myanmar), South China, the Central Andes (Bolivia, southern Peru) and Cornwall, UK. Primary tin ore deposits are part of magmatic-hydrothermal systems invariably related to late granite phases (tin granites, pegmatites, tin porphyries), and may become dispersed by exogenic processes and then eventually form placer deposits within a few km from their primary source, due to the density of cassiterite, its hardness and chemical stability. Alluvial placer deposits were usually the starting point for tin mining, and have provided at least half of all tin mined. The small-volume and late granite phases in spatial, temporal and chemical relationship to tin ore deposits are highly fractionated. Systematic element distribution patterns in these granite phases and their associated much larger multiphase granite systems suggest fractional crystallization as the main petrogenetic process controlling magmatic evolution and magmatic tin enrichment. Oxidation state controls the bulk tin distribution coefficient, with low oxidation state favoring incompatible behavior of divalent tin. Low oxidation state is also mineralogically expressed by accessory ilmenite (FeO TiO_2) as opposed to accessory magnetite (FeO Fe_2O_3) in more oxidized melt systems. This difference in the accessory mineralogy and hence metallogenic potential (tin-bearing ilmenite-series versus barren magnetite-series granites), can be easily detected in the field by a hand-held magnetic susceptibility meter. The hydrothermal system is a continuation of the magmatic evolution trend and necessary consequence of the crystallization of a hydrous melt. The exsolved highly saline aqueous fluid phase, enriched in boron and/or fluorine plus a wide metal spectrum, can be accomodated and stored by the intergranular space in crystallized melt portions, or accumulate in larger physical domains, accompanied by focused release of mechanical energy (brecciation, vein formation), dependent on emplacement depth (pressure). The hydrothermal mobility of tin is largely as Sn^{2+}-chloride complexes; the precipitation of tin as cassiterite involves oxidation. Tin typically characterizes the inner high-temperature part of much larger km-sized zoned magmatic-hydrothermal systems with the chemical signature Sn-W-Cu-As-Bi in the inner part (greisen, vein/stockwork/breccia systems, skarn) and a broader halo with vein- or replacement-style Pb-Zn-Ag-Sb-Au-U mineralization of lower temperature. This zoning pattern may also occur telescoped on each other. Active continental margins are the favorable site for both copper (−gold) and tin (−tungsten) systems. However, the narrowly segmented metal endowment and the episodic nature of ore formation suggest additional controls. These are the build-up of a subduction-derived metal and fluid inventory in the lower continental crust by flat-slab subduction (very little magmatism) for copper-gold in the main arc, followed by large-scale intracrustal melting during mantle upwelling in the back arc for tin (chemically reduced reservoir rocks) and/or tungsten mineralization (less sensitive to oxidation state).

1. Introduction

Bronze, the alloy of copper and tin, made tin a then "strategic metal" about 5000 years ago in the beginning of the Bronze Age. Tin remained a big metal in the industrial revolution, together with steel, copper, iron and aluminum. Over the last decennies, there is a renaissance of tin with the rapid development of the electronics industry where about 50% of the current tin production is used as (lead-free) solder. There are more and more high-tech applications of tin alloys, such as in superconducting magnets, advanced solar cells and liquid-crystal displays. Tin has been assessed as a medium-scale "critical metal" essential for the transition to a low-carbon economy and is within the ten most important metals associated with key decarbonization technology (Moss et al., 2013).

* Corresponding author.
E-mail address: bernd.lehmann@tu-clausthal.de.

https://doi.org/10.1016/j.lithos.2020.105756

The global tin mine production is currently about 300,000 t Sn/year, with Indonesia and China dominating, and Myanmar on a par with these two countries since a few years. The global cumulative historic tin production can be estimated to about 27 Mt Sn (up to 2020, updated from Lehmann, 1990). More than 99% of this tin production is from ore deposits directly (primary deposits) or indirectly (placers) related to granitic rocks, i.e. granites and their volcanic and subvolcanic equivalents. A small quantity of tin is or was recovered as a by-product of mining of base-metal massive sulfide deposits (such as Kidd Creek, Canada, or Neves Corvo, Portugal).

Only four well-defined regions account for about 85% of the cumulative historic tin mine output. These are (Fig. 1):

1. The SE Asian tin belt (Myanmar, Thailand, Malaysia, Indonesia) with a 40–45% share of the total world tin production.
2. The South China tin province (20%).
3. The Central Andean tin belt (Bolivia and southernmost Peru) (14%).
4. The Cornwall tin province (7%).

These regions also account for about 85% of the current global tin mine production and two thirds of the tin reserves (USGS, 2020). There are a number of discoveries and projects in development which will increase the proportion of tin mined from other parts of the world, such as the Syrymbet deposit in northern Kazakhstan and the Deputatskoe deposit in Yakutia, NE Russia, with more than 200,000 t Sn content each, or several Precambrian tin deposits under development in eastern DR Congo. For details see the World Tin and Tungsten Deposit database by Sinclair et al. (2014) and Elsner (2014).

About 90% of the historic hard-rock and alluvial tin production is related to primary tin ore deposits ≤350 Ma in age. This is a situation similar to and even more pronounced in molybdenum porphyries, copper porphyries and epithermal Au—Ag ore systems, and results from the dominant geotectonic setting in active continental margins with relatively limited survival time of shallow rocks in uplift regions. The important control of level of erosion is demonstrated by the SE Asian tin province in which the primary Mesozoic tin ore deposits are preserved only as relics and are mostly in an early state of erosional dispersion, i.e. in Cenozoic placer deposits.

Placer deposits, i.e. secondary tin deposits in surface sediments, are historically the starting point of tin mining, and still today provide nearly half of all tin production (Fig. 2). The only economically important tin mineral is cassiterite (SnO_2), which is a heavy mineral (7.15 g/cm^3) and mechanically and chemically resistant. Therefore, cassiterite becomes enriched in heavy-mineral accumulations where the transporting velocity of running water changes, such as at meanders, waterfalls, or irregular bedrock surfaces. A classic example are the "pinnacle" limestones of the Kinta Valley in Malaysia, where cassiterite washed out from eroded tin lodes in Triassic granites along the valley shoulders is enriched in the bottom of the valley on irregular Permian limestone karst surfaces (Ingham and Bradford, 1960). The alluvial sediments of this valley of about 60 km length and 5–20 km width have provided about 1.5 million tonnes (Mt) Sn during more than 100 years of mining until the sharp decline of tin production in the 1980s. Interestingly, there are only small relics of primary tin deposits preserved, similar to the situation on and around the Indonesian tin islands (Bangka, Belitung) in the Sunda shelf.

Nearly all of the currently mined tin is from emerging and developing countries. A characteristic feature of the tin mining industry is the significance of artisanal and small-scale mining which contribute about 40% to the global tin market (Elsner, 2014), mainly in Myanmar, Indonesia, Laos, Vietnam, DR Congo, Rwanda, Nigeria, and partly in Brazil and China.

2. Historical background: Early and still valid ideas

Tin provinces are one of the best examples of metallogenic provinces. They define belts on a 100- to 1000-km scale. Inside tin provinces, the association of tin ore deposits with granitic rocks has long been known. Very early studies, before even the term "granite" was established, already emphasize the association of tin and quartz-rich rocks (Rößler, 1700). Humboldt (1823) introduces the term "tin granite" as opposed to "normal granite" in the first edition of his book on global comparative geology, written in French: "granite stannifère" versus "granite primitif". A first comprehensive treatise on the ore geology of tin and at the same time the first scientific theory of magmatic-hydrothermal ore formation in general is given by Beaumont (1847), helped by the experimental work of Daubrée (1841). Essential findings are:

- Tin ore deposits are associated with granites.
- Tin ore deposits are located preferentially in apical portions of granites and their immediate country rocks. Daubrée (1841) had already pointed to the fact that tin deposits in Cornwall, in the Bretagne and Erzgebirge are always confined to a zone ≤500 m from the granite contact.
- Tin ore deposits are often associated with individual granite bodies (sub-intrusions) pointing out of larger batholiths: "les roches stannifères sont souvent des masses détachées qui ont pointé en dehors des grandes masses granitiques" (Beaumont, 1847, p. 1302).
- The tin-ore host rocks are particularly rich in quartz, tourmaline and fluorine-bearing minerals, a feature which relates to the mining

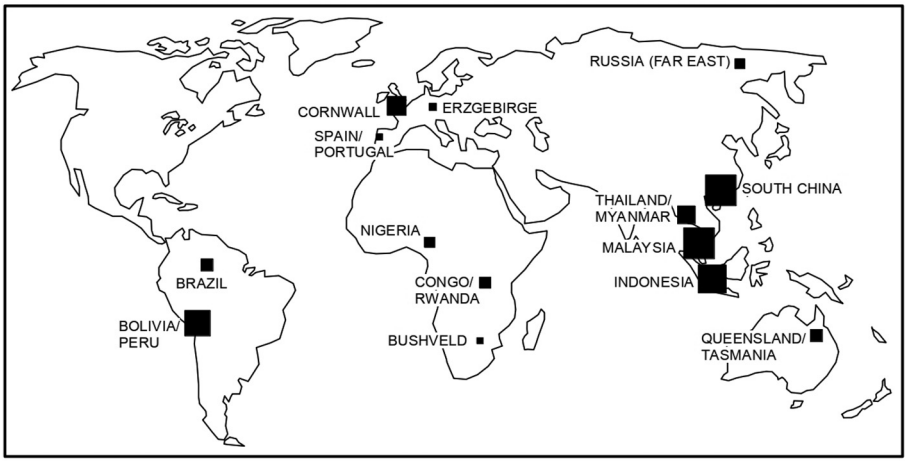

Fig. 1. Global distribution of major tin provinces. Area of black squares is proportional to total cumulative historic tin production of about 27 million tonnes (Mt) tin metal until 2020 (updated from Lehmann 1990). Note that the current tin mine production is mainly from Indonesia (25 %), China (25 %), Myanmar (17 %), and Peru, Bolivia, Brazil (5-6 % each) (USGS, 2020).

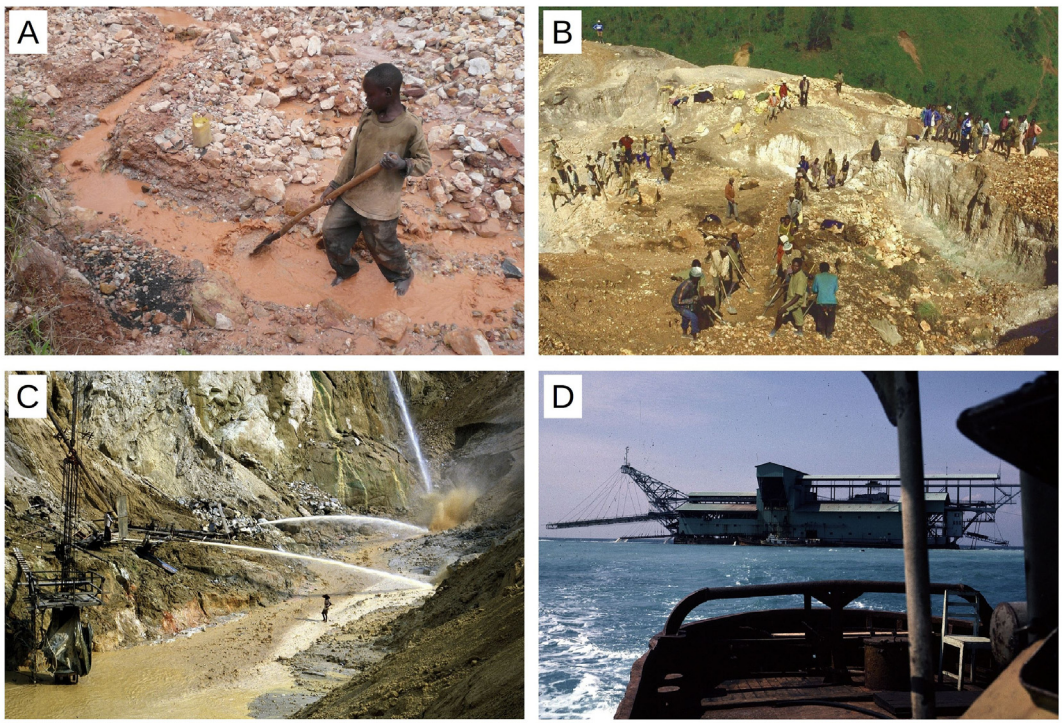

Fig. 2. About half of all tin mined (both historically and present-day) is from placer deposits, and a significant part of this placer tin mining is done by artisanal miners. The photographs show a number of variants of placer mining. A: Boy panning alluvial cassiterite with a shovel in the Gatumba district, Rwanda; B: Ground sluicing at the Kabarore Sn-Ta pegmatite, Burundi; C: Monitoring and gravel-pump mining at the Chenderiang tin mine, Kinta Valley, Malaysia; D: Deep dredging with a bucket-line tin dredge near Bangka Island, Indonesia. Photographs by Bernd Lehmann.

term of "greisen", a coarse-grained quartz-muscovite rock without feldspar which is typically associated with tin mineralization (Goethe, 1814, p. 66).
- Tin granites are anomalous in texture and composition: "des monstruités de granite" with a "caractère ultragranitique" (Beaumont, 1847, p. 1303).

Daubrée (1841) and Beaumont (1847) define tin granites as granitic rocks in which the metals of the "tin family" are particularly abundant, i.e. Sn, F, B, P, As, W, Mo, Fe, Li, Rb, Cs. The typical kaolinization in tin granites is interpreted by Daubrée (1841) as a result of hydrothermal alteration by acid fluids. The formation of tin ore deposits is explained by Beaumont (1847) by the action of circulating fluids which leach the ore components from the wall rock. The possibility that water and other volatile components may depress the solidus of a granitic melt is also discussed, and Beaumont (1847) speculates that tin granites possibly solidify at lower temperatures than normal granites.

Cotta (1859, p. 680) stressed the important fact that granite magmatism is only exceptionally accompanied by tin mineralization: "... not everywhere where granitic rocks are found, can tin ore be expected in the contact zones. The occurrence of granitic rocks together with tin ore is an exception, whereas the occurrence of tin ore together with granitic rocks is a rule" (translated from German).

These early observations provide the basis for subsequent investigations which refine the geological-mineralogical-geochemical framework of tin deposits. Modern overviews of the geology of tin ore deposits are given in Taylor (1979), Lehmann (1990) and Černý et al., (2005). The classic model is condensed in Fig. 3 with the major ingredients: (1) Multiple intrusion sequence and association of magmatic-hydrothermal tin mineralization to minor late-stage granite phases in apical portions; (2) Post-magmatic hydrothermal alteration associated with tin-bearing aqueous fluid systems, with greisen as a special expression of acid feldspar-destructive hydrothermal alteration and formation of coarse-grained quartz-muscovite±tourmaline±fluorite/topaz±cassiterite rock. Stockscheider, i.e. pegmatitic (coarse-grained granite) domains may occur at the granite/country rock contact. The model is focused on fracture-controlled vein-style tin mineralization, but there may also be reactive Ca-Mg-rich country rocks (basalt, dolomite/limestone) where skarn and carbonate replacement tin mineralization occur. And, at higher confining pressure, where late and highly evolved melt phases can keep large amounts of water in solution in a semi-closed system, rare-metal pegmatites may form, with a metal spectrum of Ta-Sn-Be-Li-Cs-Rb (Černý, 1991).

3. Global geochemical framework

The geochemical evolution of tin and some other elements during the Earth's history is schematically depicted in Fig. 4, and is first controlled by volatility (vapor-solid fractionation) and siderophile behavior (metal-silicate fractionation) during the proto-Earth evolution. The volatility of tin (50% condensation temperature at 10^{-4} bar total pressure: 720 K) is distinctly different from the volatility of the ore-paragenetically related elements W, Mo, or Ta (50% condensation temperatures at 10^{-4} bar total pressure: >1400 K). This results in a drastic decrease of tin content from about 1.8 ppm in condensed average solar material (as seen in C1 chondrites) to about 0.4 ppm in bulk Earth and 0.13 ppm in the primitive mantle.

The elements Sn and W (moderately siderophile), and Mo (strongly siderophile) partition preferentially into the core, which leaves the primitive mantle depleted in these elements when compared to solar composition. The refractory and lithophile Ta is affected neither by volatile depletion nor by substantial partitioning into the core, and follows a continuous enrichment trend during both cosmochemical and geochemical evolution. Archean crust formation by crystal-liquid fractionation of mantle material and dominance of intracrustal fractionation in the Proterozoic/Phanerozoic lead to the present-day tin distribution

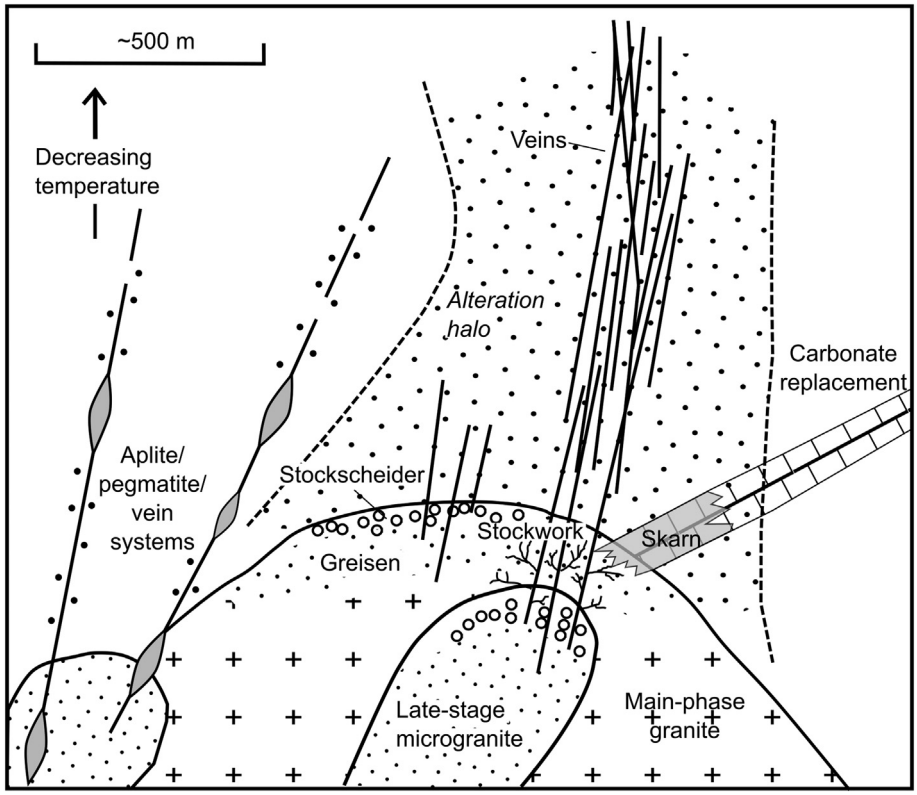

Fig. 3. Classic model of primary tin ore deposits related to magmatic hydrothermal systems set up by late granite phases with tin mineralization on top of the intrusive sequence (modified from Černý et al., 2005).

with about 1.1 ppm Sn in the lower continental crust and about 2.5 ppm in the upper continental crust (Lehmann, 1990). These numbers are within the error margin of more recent data compilations (Rudnick and Gao, 2003).

4. Geochemical specialization of tin granites

The petrological particularity of tin granites was noted very early on by Beaumont (1847) on the edge between fact and intuition. Systematic geochemical campaigns in the USSR provided a robust basis to define the geochemical specialization of tin granites as opposed to non-tin granites based on whole-rock tin content (Barsukov, 1957, p. 41): "... granitic massifs not associated with tin ores, while not differing substantially in age or mineralogical composition from tin-bearing granites, do contain tin in amounts of 3-5 ppm, which is equivalent to the Clarke of tin. Massifs, carrying tin ores in varieties unaltered by postmagmatic or contact-metamorphic processes, contain tin in somewhat larger amount - four to five times the Clarke of tin or 16 to 30 ppm (usually 18-26 ppm). Consequently, in the case of tin-bearing granites we can speak of a specialization of the granitic magma from which a given intrusive rock has solidified. Tin-bearing granites are characterized by higher tin contents in those varieties that have not been altered by contact- or postmagmatic processes". Note that "Clarke" is a historic term which refers to the average abundance of an element in the upper continental crust.

This simple but essential relationship provides the starting point for a qualitatively new period of research on tin deposits, which focusses on geochemical evolution paths in the granitic host environment. Systematic tin distribution patterns allow insight into the evolution of tin during both magmatic and hydrothermal stages and give direct information which is more obliterated in the comparable environments of copper or molybdenum deposits also associated with felsic magmatism (copper/molybdenum porphyries).

The geochemical tin specialization of tin granites is accompanied by characteristic elemental enrichment and depletion patterns. Besides the often anomalously high boron and/or fluorine contents in tin-bearing systems (noted early on by Daubrée, 1841), tin granites, when compared to average granitic rocks, are enriched in lithophile elements such as Rb, Cs, Li, Th, U, Nb, Ta and W, and are depleted in elements which are compatible with the granitic main mineral components such as Sr, Eu, Ba, Ti, Co and Ni. Trace element patterns in tin granites as well as the petrochemical equilibration to their mostly high intrusive level at 1 ± 1 kbar (minimum melt composition) point to the important role of fractional crystallization during the magmatic evolution.

There is the peculiar feature in some tin provinces that there are several episodes of tin mineralization within the same area. For instance, the Central Andean tin province has granite magmatism and associated tin deposits of Upper Triassic age in the northern part (Cordillera Real) and superimposed granite and porphyry magmatism with associated tin deposits of Miocene age over the full range of the tin belt. This phenomenon of recurrent metallogenic epochs has been called "étagement temporel" by Routhier (1967, 1983), and was intuitively explained as remobilization of a pre-existing regional tin anomaly (Schneider and Lehmann, 1977; Schuiling, 1967). This concept has recently been revived by Romer and Kroner (2015, 2016) who argue for a source control of tin provinces in the sense of sedimentary tin enrichment in the thick sedimentary sequences along continental margins. However, such sedimentary tin enrichment has never been sufficiently documented, and the magmatic fractionation trends leave little room for geochemical heritage of a regional tin anomaly (Lehmann, 1982). Interestingly, a (probably exotic) case of inheritance of cassiterite in granitic magma, comparable to zircon, has recently been observed in Neoproterozoic granite with xenocrystic zircon and cassiterite of Paleoproterozoic age which also attests to the extraordinary resistivity of the U—Pb system in cassiterite (Neymark et al., 2020). Such an inheritance is probably possible only in magnetite-series granites which have a low solubility

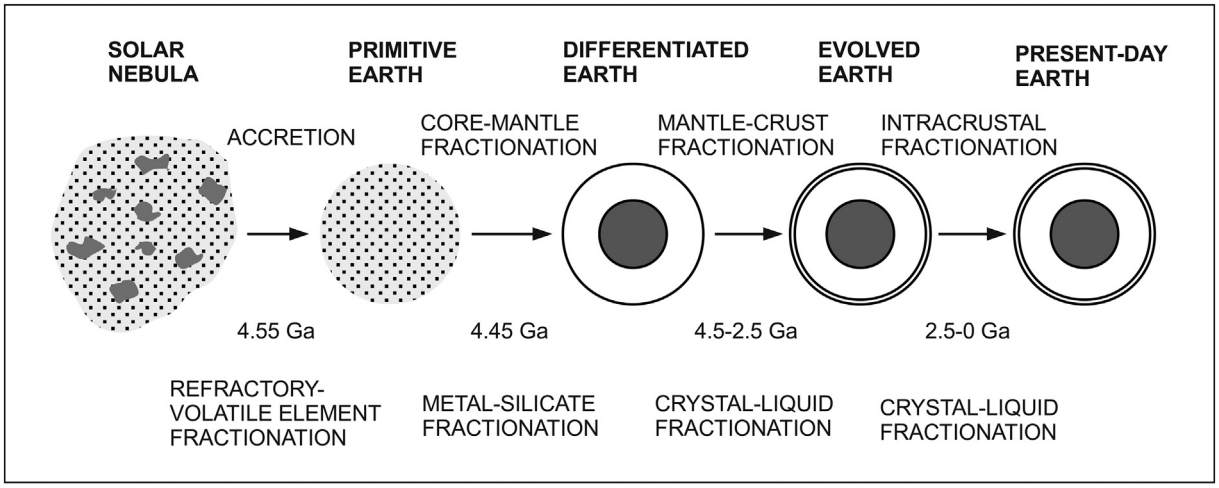

	C1 CHONDRITES	BULK EARTH	PRIMITIVE MANTLE	BULK CRUST	LOWER CRUST	UPPER CRUST
24 Cr	2660 ppm	4120 ppm	2625 ppm	135 ppm	215 ppm	92 ppm
29 Cu	126 ppm	31 ppm	30 ppm	27 ppm	26 ppm	28 ppm
42 Mo	0.93 ppm	2.35 ppm	0.05 ppm	0.8 ppm	0.6 ppm	1.1 ppm
50 Sn	1.72 ppm	0.39 ppm	0.13 ppm	1.7 ppm	1.1 ppm	2.1 ppm
73 Ta	0.014 ppm	0.023 ppm	0.037 ppm	0.7 ppm	0.6 ppm	0.9 ppm
74 W	0.093 ppm	0.18 ppm	0.029 ppm	0.7 ppm	0.5 ppm	1.9 ppm
78 Pt	0.99 ppm	1.67 ppm	0.007 ppm	0.0015 ppm	0.0027 ppm	0.0005 ppm
79 Au	0.14 ppm	0.26 ppm	0.001 ppm	0.0013 ppm	0.0016 ppm	0.001 ppm
82 Pb	2.5 ppm	0.115 ppm	0.15 ppm	11 ppm	4.3 ppm	17 ppm
92 U	0.008 ppm	0.014 ppm	0.02 ppm	1.3 ppm	0.28 ppm	2.8 ppm
Rb/Sr	0.295	0.032	0.028	0.15	0.03	0.32

Fig. 4. Fractionation pattern of some elements during Earth's history (modified from Lehmann, 1990).

of tin, and are themselves non-tin granites (see below). The general phenomenon of recurrent metallogenic epochs is also seen in the distribution of porphyry copper deposits in the Andes and southwestern North America with copper mineralization repeatedly from the late Paleozoic to Tertiary (Sillitoe, 2012). It is likely that this pattern reflects broad evolutionary orogenic cycles with interchanging episodes of slab steepening and flattening (Haschke et al., 2002) and/or crustal thickening and delamination (DeCelles et al., 2009). The South China tin province is another example of recurrent tin mineralization, with five episodes of tin mineralization comprising Neoproterozoic, Silurian, Triassic, Jurassic and Cretaceous tin deposits (Mao et al., 2013, 2019; Zhang et al., 2019). The geotectonic situation for the various tin granite events is much debated and waits for a metallogenic synthesis in a plate-tectonic framework.

The geochemical definition of tin granites by Barsukov (1957) based on tin abundance levels is commonly used and mostly valid. A more general definition is preferred here which takes into account the occasionally drastic hydrothermal tin depletion in tin granites: Tin granites are granitic rocks for which spatial, temporal and chemical relations point to a causal association with tin deposits.

A definition of tin granites must inherently be arbitrary, because those granite phases immediately associated with tin mineralization are parts of much larger composite granitic intrusions of the same petrochemical suite. Granite plutons in tin provinces are circular or elliptical bodies (usually elongated along regional strike) ranging from a few km to several tens of km in diameter, with, in general, high intrusion level. They are often assembled in such close proximity that they coalesce or can reasonably be inferred to coalesce into batholiths of regional extent (in tin provinces, for example, the Cornubian batholith, the Erzgebirge batholith, the Main Range batholith in Malaysia, etc.).

In a generalized picture which is in accordance with many situations in tin provinces, the plutons consist dominantly of coarse- to medium-grained K-feldspar megacrystic biotite monzogranite which is intruded by one or several later granite phases with a great textural variety. These subintrusions range from microgranites to aplite-pegmatite systems to granite porphyries. Such granite variants often occur in marginal or apical zones within plutons, but may also form the major outcrop area in particular situations with a high erosion level. They are geochemically more evolved than their parental granite and are affected by processes of pervasive microbrecciation and fluid overprint. Hydrothermal tin-tungsten ore systems are centered on these late and small granite phases.

However, this general situation may become more complicated, in particular in high-level intrusive/porphyry systems which may represent only the small upper part of a hidden zoned magma chamber. Such a situation applies to the Cenozoic Central Andean tin province, for example. The Bolivian tin porphyries have rhyodacite/latite composition and are much less fractionated than expected for a tin granite system. Nevertheless, these porphyries represent some of the most important tin deposits on Earth, such as Llallagua, also known as Catavi and Siglo XX, with historic production and resources on the order of 1 Mt Sn. The answer here is given in melt inclusions in quartz phenocrysts (Dietrich et al., 2000) and in the glass matrix of nearby coeval ash-flow tuffs (Pichavant et al., 1988; Morgan, 1998; London et al., 1989) and rhyodacite dikes (Sandeman and Clark, 2003). Both the melt inclusions, the rhyolite obsidian and groundmass glass in rhyodacite are highly fractionated, and attest to shallow-crustal hybridization of highly evolved silicic melt with mafic melt, or a zoned magma chamber as proposed by Hildreth (1981). There is increasing evidence that magma chambers in the sense of melt-dominated bodies occupy

only the top of much larger transcrustal magmatic systems. The deeper parts of these systems are probably largely in a crystalline state (mush) and melt may move upward through compaction-driven melt segregation from vertically extensive storage regions (Cashman et al., 2017; Sparks et al., 2019).

Tin granites are often peraluminous (prior to the often widespread muscovitization which produces a hydrothermal peraluminous overprint), and their primary peraluminous nature relates to a general S-type character due to partial melting of pelitic source material in a post-collisional environment (Sylvester, 1998). The pelitic source material is seen in specific isotope signatures (O, Hf, Nd, Sr), but also reflected in elevated boron contents of the melts and associated hydrothermal systems with abundant tourmaline (Lehmann et al., 2000b). This situation seems to apply for many granites in the major tin belts, such as the Southeast Asian tin belt (Cobbing et al., 1986; Yang et al., 2020), parts of South China (Mao et al., 2019), the Central Andean tin belt (Ericksen, 1990; Lehmann et al., 1990), and Cornwall (Jackson, 1979; Müller et al., 2006). However, there are many exceptions documented, such as the Phuket Supersuite in Thailand where the less evolved members consist of slightly metaluminous I-type hornblende granite (Pollard et al., 1995), or the Erzgebirge granite suites in Germany and Czech Republic (Breiter, 2012). There are examples of anorogenic tin granites of A-type affinity, such as in the alkaline ring complexes in Nigeria (Girei et al., 2019), the granites of the Bushveld Igneous Complex (Vonopartis et al., 2020), or parts of South China (Mao et al., 2019). The common feature of these alkaline granites is their advanced degree of fractionation and metasomatic overprint which makes it difficult to apply source-diagnostic discrimination schemes. Nevertheless, extended fractionation lines and radiogenic isotope signatures imply a significant mantle component in these granites, plus variable crustal assimilation.

5. The magmatic system

The element pattern of any igneous rock in the upper continental crust is invariably affected by postmagmatic aqueous alteration processes. This hydrothermal overprint will affect all elements soluble in water at high to low temperature. There are two metals which are particularly insoluble in hot water. These are titanium and, even more so, tantalum. The extremely low aqueous solubility of tantalum is the reason why Ta deposits only form in the magmatic environment, such as Ta pegmatites. We therefore use Ti and Ta as indicators of the magmatic evolution of felsic igenous rocks where Ta is generally incompatible (enriched in residual melt) and Ti is generally compatible (incorporated in biotite and other early crystallizing Ti-bearing minerals) (Lehmann, 1990). Note, however, that the behavior of both Ti and Ta depends on the melt composition. Titanium in mafic melt systems, such as basalt, is incompatible until magnetite crystallization, while the incompatible behavior of Ta is limited by accessory phases (ilmenite, rutile, titanite) which, however, are usually quantitatively insignificant (Stepanov et al., 2014), The Ti—Ta plot of Fig. 5 shows the typical magmatic evolution in various multi-phase granite suites. The linear correlation of whole-rock titanium and tantalum content in the log-log plot is in accordance with the model of fractional crystallization during the magmatic evolution of these rocks. Mixing/assimilation processes would result in hyperbolic correlation patterns in log-log space (and linear correlation in linear space). The diagram shows average data from a very large dataset on the Erzgebirge granites (Tischendorf, 1989). These granites are mapped in detail since more than 100 years, and their temporal sequence is well established. The data distribution in Fig. 5 corresponds to the relative time sequence from oldest (and most voluminous) at low Ta and high Ti to youngest (and least voluminous) with elevated Ta and very low Ti. Tin mineralization in the Erzgebirge (and elsewehere) is always related to the youngest intrusive phase with the most advanced magmatic evolution. In fact, the two data points with the lowest Ti values correspond to the Zinnwald apogranite (200 ppm Ti) and the aplite/pegmatite system of the Ehrenfriedersdorf tin deposit (60 ppm Ti), respectively. The time interval in between the intrusion of the different granite phases is usually smaller than the error of radiometric dating. In the case of the Erzgebirge suite, the age interval is 326–320 Ma (Zhang et al., 2017). Granite suites from other parts of the world follow the same trend. The diagram also shows data from the Variscan Massif Central granites in France (Raimbault et al., 1995), the Mesozoic Border Range granites in Thailand/Myanmar (Lehmann and Mahawat, 1989), and the Late Neoproterozoic Sn—Ta apogranite of Abu Dabbab, Egypt (Lehmann et al., 2020; Zoheir et al., 2020;). These data are from individual samples, not averages from large-scale sampling as in the Erzgebirge. The diagram also shows the average from a survey of some Neoproterozoic rare-metal pegmatites in Rwanda (Lehmann et al., 2014). The composite igneous sequence can be traced back to average continental crust and is different from granitic rocks in general which are less evolved (compared to the GEOROC database).

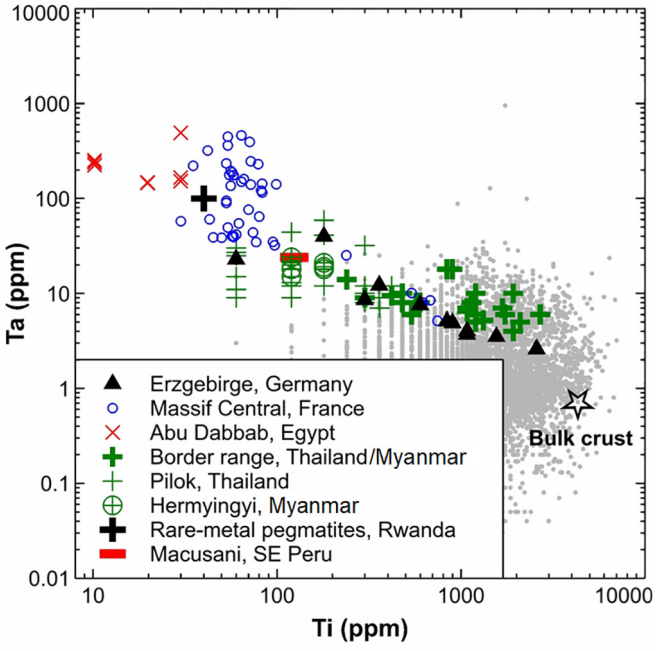

Fig. 5. Titanium versus Ta plot for various granite suites related to tin mineralization. Titanium behaves compatible in felsic igneous systems while Ta is incompatible, i.e. Ti becomes depleted during magmatic fractionation processes, while Ta becomes enriched. Both elements are largely immobile during hydrothermal overprint and therefore record best the igneous situation. The most evolved granite phases, where Ti is at trace element levels, are directly related to tin mineralization, such as in the Erzgebirge (Tischendorf 1989), Massif Central (Raimbault et al. 1995), Abu Dabbab rare-metal granite, Egypt (Lehmann et al. 2020), Border Range granites of Thailand and Myanmar including Pilok Sn granite (Lehmann and Mahawat 1989, plus unpublished data), and rare-metal pegmatites in Rwanda (average from Lehmann et al. 2014). The Macusani data from Puno, southeastern Peru, relate to highly evolved rhyolite obsidian coeval with the Miocene Bolivian tin porphyries (London and Morgan 2017; Pichavant et al. 1988). Bulk crust composition is from Rudnick and Gao (2003). The many grey dots correspond to felsic igneous rocks of >68 wt% SiO_2 from the global GEOROC data archive (georoc.mpch-mainz.gwdg.de).

The Ti versus Sn diagram in Fig. 6 shows a similar trend as in Fig. 5, but with more scatter. Titanium is used as an indicator of magmatic fractionation relatively insensitive to aqueous alteration processes. In contrast, tin is known to be quite mobile in hot water, as demonstrated by the widespread existence of hydrothermal tin deposits. Therefore, the magmatic tin distribution pattern may be affected by late- or postmagmatic alteration. The Erzgebirge reference suite defines a distinctive negative log-log correlation trend, similar to the Ti versus Ta diagram in Fig. 5. This may be due to the fact that the data points refer to averages from a large data set of samples away from ore deposits. The average of rare-metal pegmatites from Rwanda and the individual data from the Abu Dabbab apogranite in Egypt are also along the

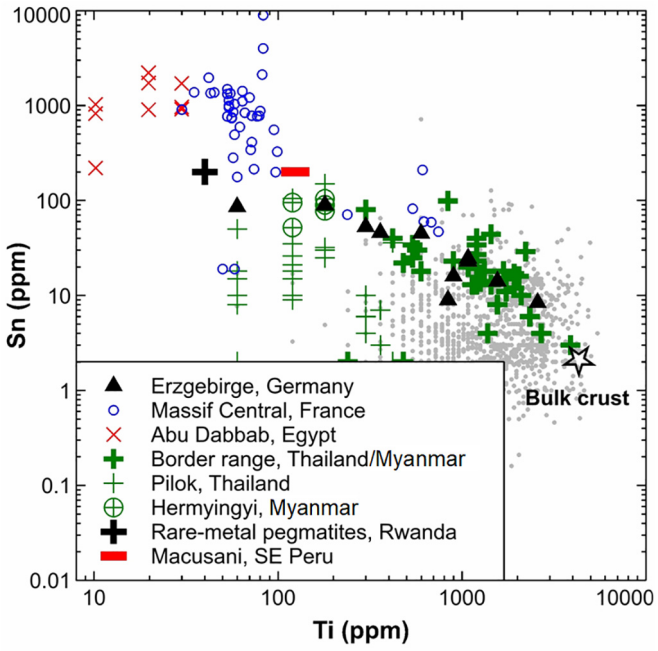

Fig. 6. Titanium versus Sn plot for various granite suites related to tin mineralization. Titanium behaves compatible in felsic igneous systems and is relatively immobile during hydrothermal processes, while tin behaves incompatible in the systems shown, but is mobile during hydrothermal overprint. The most evolved granite phases, where Ti is at trace element levels, are directly related to tin mineralization, such as in the Erzgebirge (Tischendorf 1989), Massif Central (Raimbault et al. 1995), Abu Dabbab rare-metal granite, Egypt (Lehmann et al. 2020), Border Range granites of Thailand and Myanmar including Pilok Sn granite (Lehmann and Mahawat 1989, plus unpublished data), and rare-metal pegmatites in Rwanda (average from Lehmann et al. 2014). Note that the Pilok tin granite shows a scatter distribution indicating a deficiency in tin which can be interpreted as the tin in the hydrothermal vein systems with cassiterite mineralization. Scatter is also indicated in the samples from Massif Central, France, while the tin data in the Abu Dabbab granite and in rare-metal pegmatites, Rwanda, seem to mainly represent the igneous situation. There is no significant scatter in the Erzgebirge granite suite because these data are averages for many individual samples. The Macusani data from Puno, southeastern Peru. relate to highly evolved rhyolite obsidian coeval with the Miocene Bolivian tin porphyries (London and Morgan 2017; Pichavant et al. 1988). The many grey dots correspond to felsic igneous rocks of >68 wt% SiO_2 from the global GEOROC data archive (georoc.mpch-mainz.gwdg.de).

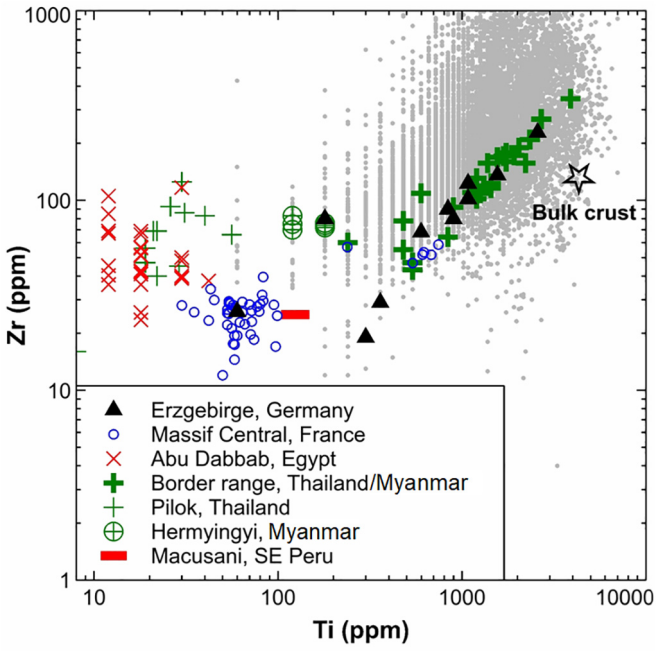

Fig. 7. Titanium versus Zr plot for various granite suites related to tin mineralization. Titanium behaves compatible in felsic igneous systems and is relatively immobile during hydrothermal processes, similar to Zr for peraluminous systems. However when zircon saturation is reached, Zr contents remain ± constant. The most evolved granite phases, where Ti is at trace element levels, are directly related to tin mineralization, such as in the Erzgebirge (Tischendorf 1989), Massif Central (Raimbault et al. 1995), Abu Dabbab rare-metal granite, Egypt (Lehmann et al. 2020), Border Range granites of Thailand and Myanmar including Pilok Sn granite (Lehmann and Mahawat 1989, plus unpublished data), and rare-metal pegmatites in Rwanda (average from Lehmann et al. 2014). The Macusani data from Puno, southeastern Peru. relate to highly evolved rhyolite obsidian coeval with the Miocene Bolivian tin porphyries (London and Morgan 2017; Pichavant et al. 1988). The many grey dots correspond to felsic igneous rocks of >68 wt% SiO_2 from the global GEOROC data archive (georoc.mpch-mainz.gwdg.de).

trend, in a more extreme tin enrichment position. These systems have disseminated tin mineralization largely confined to the granite bodies, i.e. relatively subdued hydrothermal vein systems. This is different for the samples from the Massif Central in France and the Border Range granites of Thailand/Myanmar; both areas have major hydrothermal tin vein systems. In particular, the Pilok area in Thailand within the Border Range granite domain, has extensive sheeted vein sets with hydrothermal tin mineralization, and the apparent tin deficiency displayed by the Pilok samples (Fig. 6) is likely due to the complementary tin enrichment in the associated hydrothermal vein system (Lehmann and Mahawat, 1989).

Importantly, the igneous tin enrichment trend can be traced back to Sn levels of ≤10 ppm in the least-evolved rock portions, most even down to 5 ppm Sn, as shown by Lehmann (1982) for many tin granite systems, not only the few examples in Fig. 6. The assumption that the source material of tin granite suites may already be enriched in tin beyond average crustal levels, as occasionally suggested (Romer and Kroner, 2015; Schuiling, 1967), is therefore not justified. With partial melting rates in anatectic granodiorite-granite systems in the range of 20–50% and moderately incompatible behavior of tin (D_{Sn} restite/melt = 0.5) bulk-crust material can be expected to yield partial melts with at least 5 ppm Sn, as already observed by Barsukov (1957).

For comparison with the distribution patterns of Ta and Sn, Figs. 7 and 8 show the behavior of Zr and U with respect to Ti as the common indicator of fractionation. Zirconium is relatively immobile in aqueous systems and behaves compatible in peraluminous melt systems until zircon saturation at less than 100 ppm Zr (Watson, 1979) when its concentration in the melt will remain ± constant. This pattern applies to the late-phase granites selected in Fig. 7. Much different from Zr, uranium is highly mobile in aqueous fluids, particularly under oxic conditions, and the magmatic distribution of U cannot be expected to be preserved in bulk-rock samples. Nevertheless, the data in Fig. 8 show a scatter distribution at generally elevated U levels which suggests magmatic enrichment, i.e. incompatible behavior of U during the magmatic evolution, combined with intense postmagmatic hydrothermal or low-T aqueous redistribution.

The magmatic tin enrichment trend in Fig. 6 has a slope defined by $[D_{Sn} - 1] / [D_{Ti} - 1]$ which follows from the Rayleigh fractionation law (Lehmann, 1990) (D refers to the bulk distribution coefficient Sn_{solid}/Sn_{melt}). The global comparison of different tin granite and non-tin granite sequences has shown that this slope can vary, from about −1 to 0 (Lehmann, 1982), where the slope around −1 corresponds to tin granite situations (as in Fig. 6), and the slope around 0 corresponds to non-tin granites, i.e. the majority of all granites. There is a continuum in slopes for different granitic fractionation suites (Lehmann, 1982, 1990). This finding suggests that the bulk Sn distribution coefficient can change significantly. One major control of this distribution coefficient is the oxidation state of the melt system, expressed as oxygen fugacity fO_2.

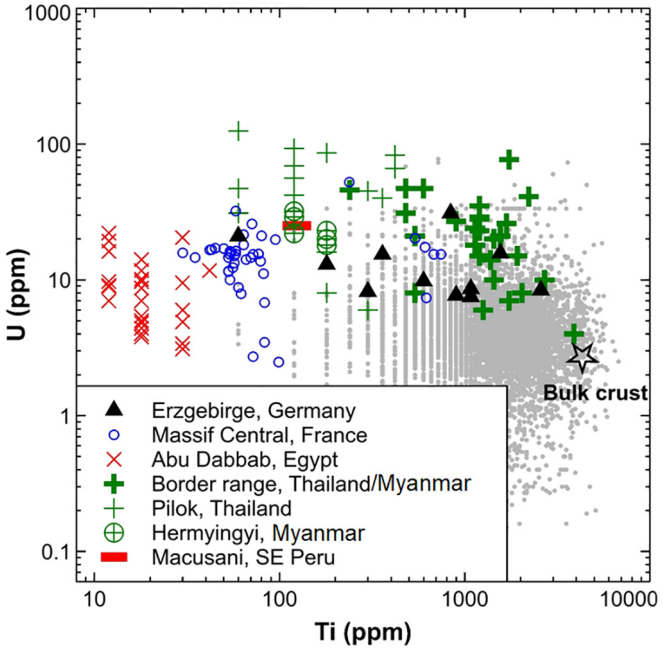

Fig. 8. Titanium versus U plot for various granite suites related to tin mineralization. Titanium behaves compatible in felsic igneous systems and is relatively immobile during hydrothermal processes. Uranium is incompatible up to uraninite saturation, and is extremely mobile in aqueous systems, particularly under oxic conditions (meteoric water). The plot shows a scatter distribution at elevated U abundance. The aqueous mobility of U largely extinguishes the magmatic enrichment pattern. The deficiency of U likely relates to hydrothermal U mineralization, typical of many tin provinces. The most evolved granite phases, where Ti is at trace element levels, are directly related to tin mineralization, such as in the Erzgebirge (Tischendorf, 1989), Massif Central (Raimbault et al., 1995), Abu Dabbab rare-metal granite, Egypt (Lehmann et al., 2020), Border Range granites of Thailand and Myanmar including Pilok Sn granite (Lehmann and Mahawat, 1989, plus unpublished data), and rare-metal pegmatites in Rwanda (average from Lehmann et al., 2014). The Macusani data from Puno, southeastern Peru. relate to highly evolved rhyolite obsidian coeval with the Miocene Bolivian tin porphyries (Pichavant et al., 1988; London and Morgan, 2017). The many grey dots correspond to felsic igneous rocks of >68 wt% SiO_2 from the global GEOROC data archive (georoc.mpch-mainz.gwdg.de).

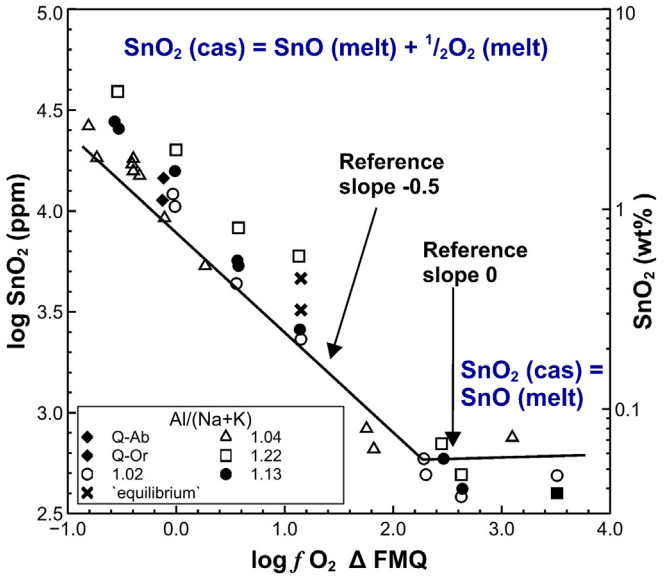

Fig. 9. Experimental log solubility of cassiterite vs. log fO_2 for peraluminous granitic melt compositions (adapted from Linnen et al. 1996, p. 4970). The experimental data follow two trends: slope − 0.5 at relatively low oxygen fugacity, and slope 0 at more elevated oxygen fugacity two orders of magnitude higher than the FMQ buffer (fayalite-magnetite-quartz). The more elevated oxidation state corresponds to typical volcanic-arc magmatism with involvement of oxidized and hydrated mantle melts, while the more reduced oxidation state corresponds to intracrustal magmatism with involvement of melts from reduced lithologies such as shale with organic carbon. The slope of −0.5 relates to the dominance of divalent tin in the melt system (m), according to the equilibrium constant for the equation SnO_2 (cassiterite) = SnO (melt) + ½O_2 with K = $[SnO] \times [O_2]^{½} / [SnO_2]$, and log K = 0.5 log$O_2$ + logSnO, i.e. logSnO = −0.5 logO_2 - logK. For tetravalent tin in the melt system the equation SnO_2 (cassiterite) = SnO_2 (melt) is independent of fO_2, i.e. slope = 0.

Experimental work by Linnen et al., (1996) showed that the solubility of cassiterite in peraluminous granitic melt strongly depends on oxygen fugacity (Fig. 9), with solubilities of several wt% Sn under the most reducing conditions. The data follow a straight line with a slope of −0.5 in a log Sn versus log fO_2 plot, as expected from the reaction.

$$SnO_2\ (\text{cassiterite}) = Sn^{2+}\ (\text{melt}) + O^{2-}\ (\text{melt}) + ½O_2 \quad (1)$$

Only at rather high oxygen fugacities – more than one log unit above the Ni-NiO buffer – cassiterite solubility becomes independent of redox conditions, since SnO_2 then dissolves as Sn^{4+} in the melt, which does not involve any change in oxidation state. Tin solubility decreases with increasing alkalinity of the melt (Bhalla et al., 2005) and in peralkaline melts tetravalent Sn seems to be dominant even at low oxidation state of the melt (Farges et al., 2006).

The experimental data confirm previous suggestions by Ishihara (1977, 1981) that tin in melt systems may exist predominantly either as Sn^{2+} (reduced systems) or Sn^{4+} (oxidized systems). Ishihara (1977) observed that tin enrichment occurs only in granites which have accessory ilmenite, while no tin enrichment is observed in granites which have accessory magnetite and associated molybdenum mineralization. He divided the granite spectrum in ilmenite-series granites (reduced) and magnetite-series granites (oxidized), and the underlying relationship between accessory mineral assemblage and oxidation state is given by:

$$3CaTiSiO_5 + 2Fe_3O_4 + 3SiO_2 = 3CaFeSi_2O_6 + 3FeTiO_3 + O_2 \quad (2)$$

$$\text{Titanite} + \text{Magnetite} + \text{Quartz} = \text{Hedenbergite (or any other silicate)} + \text{Ilmenite}$$

Tin in the divalent state, i.e. in ilmenite-series granites, behaves incompatible, whereas tin in the tetravalent state, i.e. in magnetite-series granites, behaves compatible. The reason is the close ionic radius and equal valency of Sn^{4+} and Ti^{4+}, which allow incorporation of Sn^{4+} in the early crystallizing titanium-bearing minerals, such as biotite and titanomagnetite. This situation is opposite to molybdenum, for instance, which behaves compatible in the reduced state as Mo^{4+}, leading to no or little Mo enrichment in ilmenite-series granites. But molybdenum in the oxidized state of Mo^{6+}, as in magnetite-series rocks, leads to Mo enrichment (Ishihara, 1981), such as seen in the Mo porphyries of the Colorado mineral belt, for instance, which have no tin mineralization in spite of high degree of magmatic evolution. The granite series in tin provinces are all of ilmenite-series affinity (Erzgebirge, Massif Central, Cornwall, SE Asian and South China tin belts, Central Andean tin belt in Bolivia, Central African rare-metal pegmatites, etc.). This important metallogenic feature can be verified in the field with a simple device, a portable magnetic susceptibility meter, which measures the magnetite content in a rock.

The solubility data of tin in silicic melts suggest that crystallization of magmatic cassiterite from a peraluminous melt containing tin at the ppm level is unlikely (Fig. 9). Magmatic cassiterite is particularly unlikely in low fO_2-tin granites (ilmenite series), even with tin contents of a highly fractionated melt at the 100 ppm level; but cassiterite saturation may occur in extremely fractionated pegmatite phases, particularly where there is a late-stage oxidation of the melt.

Empirical crystal-liquid distribution coefficients for tin, D_{Sn}, have been obtained by measurements of phenocrysts and groundmass in porphyritic subvolcanic/volcanic rocks in the pioneering studies of Antipin et al. (1981) and Kovalenko et al. (1986, 1988). D_{Sn} (crystal/

melt) for quartz, plagioclase, K-feldspar is always <1 and decreases with decrease in temperature. D_{Sn} (crystal/melt) for magnetite is always >1 (4–12), and independent of temperature, as for titanite (~60), and hornblende (~2). D_{Sn} (crystal/melt) for mica (biotite and muscovite) is >1 and increases with decrease in temperature. D_{Sn} (crystal/melt) for olivine and clinopyroxene is slightly less than 1, and independent of temperature.

Experimental work on tungsten solubility in granitic melts suggests that wolframite solubility is nearly independent of oxygen fugacity in the FMQ to NNO + 2 range with W^{6+} as the predominant species (Che et al., 2013). Tungsten solubility in aqueous fluids is mainly in simple tungstate compounds and the predominant species is also W^{6+} (Wood and Samson, 2000), but there are various other complexation types and the behavior of tungsten is currently not well understood (Zajacz et al., 2008). The less redox-dependent behavior of tungsten is different from tin, and may explain the large variability in the tin-tungsten ore spectrum from tin-only to tungsten-only deposits.

6. The hydrothermal system

The magmatic and hydrothermal systems in tin granite situations form a continuum characterized by complex transitional phenomena. The transitional stage begins with the differential release of a fluid phase at the solubility boundary of the melt-crystals system as a function of total pressure (level of intrusion), degree of solidification and initial fluid content and fluid composition in the melt. The transitional stage grades below the solidus into the hydrothermal stage. A consequence of fluid saturation may be fluidization of the residual magma, which may lead to the pervasive emplacement of such hydrous melt into already crystallized and consolidated granite. Disruptive, secondary porphyry textures of a wide variety may result. The mix of coarse- to medium-grained crystals in fine-grained groundmass of the same mineralogical composition was termed two-phase granite (Cobbing et al., 1986). A dynamic system composed of multiple intrusions with episodic release of mechanical energy (hydraulic fracturing) may accumulate fluids in intergranular space which on microfracturing in the local stress field may be intermittently tapped and collected on larger structures (reservoir model by Pollard and Taylor, 1986). The comagmatic fluid exsolution and accumulation on intergranular space causes chemical and textural convergence between magmatic and hydrothermal mineral formation in granitic rocks.

Supporting textural evidence for fluid exsolution can be found to some degree in any granitic intrusion. Magmatic-hydrothermal phenomena will, however, be most pronounced in strongly fractionated granites where the fluid-accommodating capacity of intergranular spaces may be exceeded. Field evidence for local fluid saturation in tin granites are aplite-pegmatite domains on a cm- to m-scale in the form of pods, lenses, pipes and veins with repetitive features of textural contrasts (fine-/coarse-grained) and mineral corrosion, and pockets on a microscopic to megascopic scale of quartz-feldspar mosaics. On the microscopic scale, there is a wide variety of textures produced by high-temperature fluid interaction (partially in equilibrium with the magmatic mineral assemblage) such as blebbing of feldspars by albite or secondary quartz, feldspar-quartz myrmekites, micrographic and symplectic intergrowths of quartz, feldspars and muscovite.

An important feature of tin systems is their igneous and hydrothermal boron (mineralogically expressed as tourmaline) and/or fluorine (expressed as topaz and fluorite) enrichment. Boron promotes higher water solubility in melts, and water content controls the amount of mechanical energy released during crystallization of residual magmas (Burnham, 1979; Pichavant, 1981). Widespread tourmaline breccia pipes and stockworks attest to the relatively high mechanical energy developed during the crystallization of B-rich magmas. This is different to the metasomatic greisen style with disseminated mineralization in F-rich environments which may reflect the relatively low amount of mechanical energy released during the crystallization of water-poor, F-bearing magmas (Pollard et al., 1987). Fluid release from within the magma provides an explanation for the fracture pattern in high-level granitic intrusions which is centered on late and most evolved intrusion phases; a situation typical of copper, as well as tin-tungsten and molybdenum porphyries/granites. There may also be an external trigger for massive fluid expulsion such as volcano collapse or earthquakes (Richards, 2018). The high salinity and stable isotope composition of early hydrothermal fluids in these deposits point to a magmatic origin of the ore fluids which during the cooling history of the magmatic-hydrothermal systems may become dominated by external (meteoric) fluids.

High-pressure experimental data on the partitioning of Sn between melt and an aqueous fluid phase are difficult to obtain due to alloying of Sn with the noble metals (Au or Pt) of the sample capsule, and the available data with D_{Sn} (aqueous fluid/melt) <1 seem to be too low, likely due to loss of tin from the charge (Keppler and Wyllie, 1991; Nekrasov et al., 1980). An experimental approach via synthetic fluid inclusions obtained D_{Sn} (aqueous fluid/melt) values of 0.1–0.5 for metaluminous melt, and values of 2–4 for peraluminous melt conditions at 700°C, 100–200 MPa and logfO_2 NNO (Duc-Tin et al., 2007). These values must be significantly higher in tin granite situations where logfO_2 can be expected to be up to two log units below the NNO buffer. Note that for a typical solubility of 5 wt% H_2O in the melt, D_{Sn} (aqueous fluid/melt) needs to be >20 to result in a net depletion of Sn in the residual melt (assuming 100% incompatibility of Sn with respect to the crystallizing solid phases).

Tin in hydrothermal solutions is mainly transported as chloride complexes (mainly $SnCl^-$ and $SnCl_2$) and its mobility is essentially controlled by temperature, salinity, pH and oxygen fugacity (Eugster, 1986; Wilson and Eugster, 1990). The optimal constellation of these parameters is given at high salinity and temperature, and low fO_2 and pH. An aqueous phase in a tin granite system (at or below the NNO oxygen buffer) at 700°C will have a tin-transporting capacity on the order of 100 ppm Sn (Fig. 10). This applies to pH conditions with feldspar stable. Lower pH at feldspar-destructive conditions on cooling will increase tin solubility by orders of magnitude. Fluid inclusions from the Huanuni tin deposit, Bolivia, which were trapped at about 380°C, have tin concentrations of about 100 ppm Sn (Müller et al., 2001). Low-pH conditions of a fluid-buffered hydrothermal evolution are possible in spatially restricted circulation systems such as quartz veins or greisen environments in which feldspar was previously destroyed.

The formation temperature of cassiterite in tin ore deposits is commonly in the range of 300–500°C as noted in the first summary study on fluid inclusions by Little (1960) and later confirmed by numerous investigations summarized in Naumov et al. (2011) and Bodnar et al. (2014). Occurrences of colloidal wood tin (hydrocassiterite) in Mexico and Bolivia seem to have formed at a temperature as low as about 150°C. Salinity data from fluid inclusions in cassiterite and associated quartz vary widely between 1 and > 50 wt% NaCl-equivalent, with a typical average range of 5–20 wt% (1–4 m NaCl) (for Bolivia: Kelly and Turneaure, 1970; Grant et al., 1977; and general review in Roedder, 1984). The ranges in homogenization temperature and salinity are roughly similar to those observed in copper porphyry systems. There is a distinct positive correlation between salinity and homogenization temperature that is commonly interpreted to represent cooling and dilution of early magmatic fluids by meteoric fluids (Bodnar et al., 2014).

Fig. 11 summarizes the typical temperature evolution and mineralogical sequence in hydrothermal tin deposits. The diagram is from the classic work by Kelly and Turneaure (1970) who studied over fifty tin and tungsten deposits in Bolivia which in spite of different ages and genetic types gave a uniform evolutionary pattern. This pattern, although in individual deposits commonly not developed in full, provides a general framework with respect to temperature and mineral association in tin ore formation.

Cassiterite precipitation according to the general equilibrium

$$SnCl^{+} + H_2O + \tfrac{1}{2}O_2 = SnO_2 + 2H^{+} + Cl^{-} \quad (3)$$

is redox- and pH-dependent and must therefore be accompanied by H^+-consuming processes and oxidation. Note that a one unit increase in pH will force cassiterite to become supersaturated by two orders of magnitude, and vice versa. A drop in temperature will decrease tin solubility by as much as one order of magnitude. Acid neutralization is most effectively achieved in carbonate rocks during the formation of skarn or sulfide replacement tin deposits by the calcite dissolution reaction.

$$CaCO_3 + H^{+} = Ca^{2+} + HCO_3^{-} \quad (4)$$

which, together with (3) gives:

$$SnCl^{+} + 2CaCO_3 + H_2O + \tfrac{1}{2}O_2 = SnO_2 + 2Ca^{2+} + 2HCO_3^{-} + Cl^{-} \quad (5)$$

Feldspar-destructive wall rock alteration is the dominant H^+-consuming reaction in non-carbonate rocks in which muscovitization of alkali-feldspar is an important feature, such as:

$$3(Na,K)AlSi_3O_8 + 2H^{+} = KAl_2AlSi_3O_{10}(OH)_2 + 6SiO_2 + 2Na^{+} \quad (6)$$

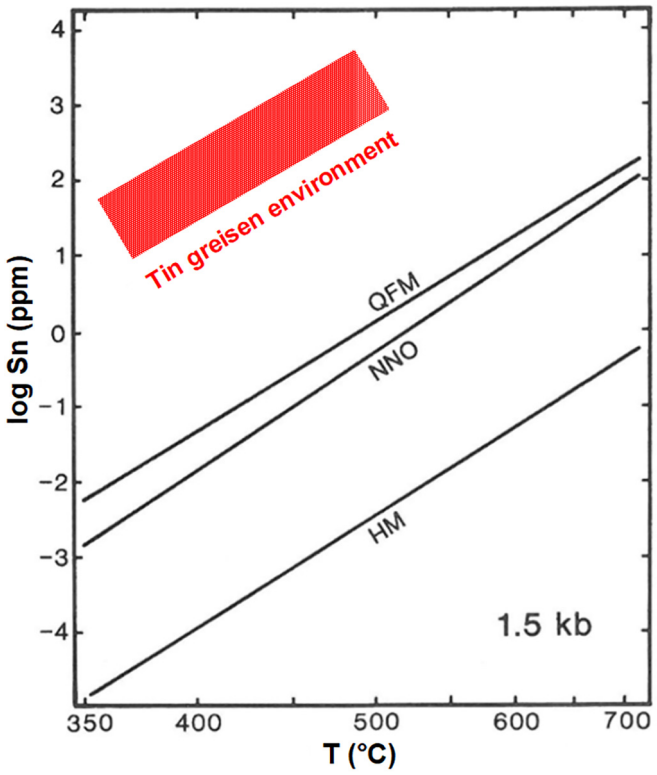

Fig. 10. Log solubility of Sn in ppm in aqueous fluids at 1.5 kb as a function of temperature and fO_2 defined by the experimental QFM (quartz-magnetite-fayalite), NNO (Ni-NiO) and MH (magnetite-hematite) oxygen buffers. The assemblage K-feldspar + quartz + muscovite defines near-neutral pH, chloride molality is 2 m, K/Na is 0.15. Tin solubility is overall relatively low, but two orders of magnitude higher for reduced conditions (QFM) compared to oxic conditions (HM). An acid fluid (greisen environment) with low pH will have a tin solubility orders of magnitude higher because of the inversely proportional relationship of $\log Sn \propto -2pH$ (see text, eq. 3). Adapted from Wilson and Eugster (1990, p. 192). Note that the cassiterite solubility in this plot is modeled for Sn^{2+}-chloride species only. Aqueous Sn^{4+}-chloride species are indicated by recent experimental work by Schmidt (2018) which was, however, under unconstrained conditions of the oxidation state. Experimental work by Duc-Tin et al. (2007) indicates tin solubility of 100–800 ppm Sn in moderately saline (5–35 wt% NaCl) fluid at 700°C and at the NNO buffer.

which, together with (3) gives:

$$SnCl^{+} + 3(Na,K)AlSi_3O_8 + 2H_2O = SnO_2 + KAl_2AlSi_3O_{10}(OH)_2 + 6SiO_2 + 2Na^{+} + Cl^{-} \quad (7)$$

Cassiterite is the only important economic tin mineral. However, during the sulfide stage at decreasing temperature, stannite [Cu_2FeSnS_4] typically occurs. The formation of both minerals requires the oxidation of Sn^{2+} to Sn^{4+}. Recent work shows that the tin isotope composition in stannite is consistently more fractionated toward lighter isotope values than that of paragenetically earlier cassiterite, and this isotopic shift is likely attributable to the fluid evolution with precipitation of early heavy-Sn-enriched cassiterite and precipitation of lighter Sn in the later formed stannite from isotopically fractionated solutions (Brügmann et al., 2017; Yao et al., 2018).

7. Metallogenic model

Tin ore deposits are part of fossil hydrothermal systems centered on highly evolved late phases of extended granitic fractionation suites. According to systematic trace element distribution patterns in these subunits and in associated larger granite systems, fractional crystallization seems to be the dominant petrogenetic process controlling magmatic evolution. Convective fractionation, i.e. convection of fluid away from crystals during sidewall crystallization, could provide an effective crystal-melt separation mechanism in upper crustal melt domains (Sparks et al., 1984), although combined magma compaction and reactive melt flow may be the dominant process in the underlying transcrustal magma reservoir region (Sparks et al., 2019). The multiphase nature of the intrusion systems and their systematic enrichment patterns in incompatible trace elements toward the youngest and volumetrically smallest phases point to episodic tapping of an increasingly fractionated and buoyant magma chamber below the gradually deepening solidification front.

Strontium and Nd isotope data indicate for most tin granite suites an origin predominantly by partial melting of crustal material; in some tin provinces a substantial mantle component seems to be involved. The starting material of the granitic fractionation suites has no anomalous contents in tin as compared to average pelitic material. The tin specialization of tin granites is a consequence of their magmatic evolution, and crustal thickness may be an important parameter in influencing the magma residence time and its spatial evolution. This is suggested by the more continental setting of tin granite systems (or of any evolved silicic melt systems) as compared to the chemically less evolved copper porphyries.

Degree of fractionation and oxidation state are the two parameters of prime importance for magmatic tin enrichment in granite suites, and have a regional control over the formation of tin provinces. A low oxidation state is required for the presence of dominantly Sn^{2+} in the melt (incompatible) compared to Sn^{4+} (compatible). Low oxygen fugacity in granitic melt could be provided by source material with high Fe^{2+}/Fe^{3+} ratio and/or high carbon or S^{2-} content. Pelitic sedimentary sequences on the order of 10 km of stratigraphic thickness are typical of the basement of many tin provinces (SE Asia, Bolivia, Cornwall, Portugal). Pelitic source rock material makes little difference to the magmatic tin distribution patterns in tin granites as compared to other source rocks. However, the extreme boron enrichment of many tin granite systems likely reflects the distinct boron enrichment of average shale (100–200 ppm B) as compared to bulk crust (10 ppm B) (Lehmann et al., 1990), whereas the corresponding tin data are 2.5 ppm (bulk crust) and 3–5 ppm (shale) (Taylor and McLennan, 1985). An indication for pelitic source rock material in most (but not all) tin granite suites is the generally peraluminous S-type character of these granites, which contrasts with I-type fractionation suites associated with F-dominated molybdenum (but also tin) ore systems.

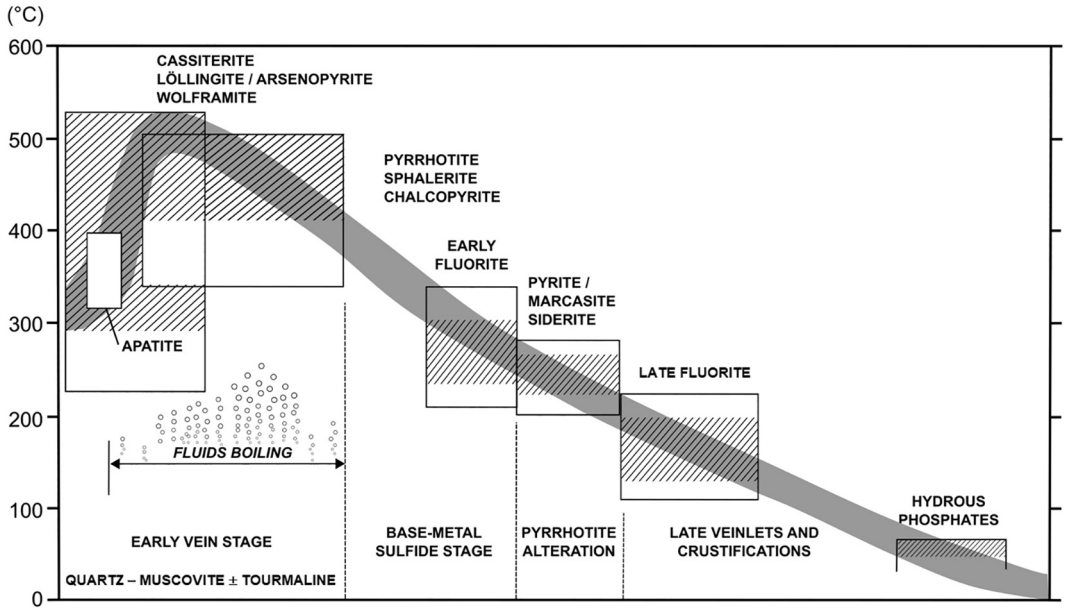

Fig. 11. Generalized temperature evolution of tin deposits in the Bolivian tin belt, derived from fluid inclusion data and from mineral equilibria (Kelly and Turneaure, 1970, p. 673). A typical feature of these relatively reduced hydrothermal systems is the formation of pyrrhotite as the first iron sulfide mineral which later is transformed to pyrite/marcasite and siderite, or completely extinguished by pyrite blastesis.

The hydrothermal tin ore system is a continuation and result of the magmatic evolution trend, with shallow intrusion level providing high permeability and fluid circulation. The exsolution of a chloride-bearing fluid phase from a crystallizing granitic melt is the necessary consequence of anhydrous crystallization of a hydrous melt (Holland, 1972). The exsolved fluid phase can be accommodated and stored by the intergranular space in little fractionated magma portions. In higher fractionated melt portions, larger physical domains of a fluid phase will form during solidification, accompanied by focussed development of mechanical energy during retrograde boiling (Burnham, 1979). The symmetry of structurally controlled permeability patterns centered on apical portions of highly evolved granite stocks argues for such a situation which is particularly developed in subvolcanic settings (porphyry-type stockworks, pervasive brecciation, breccia pipes).

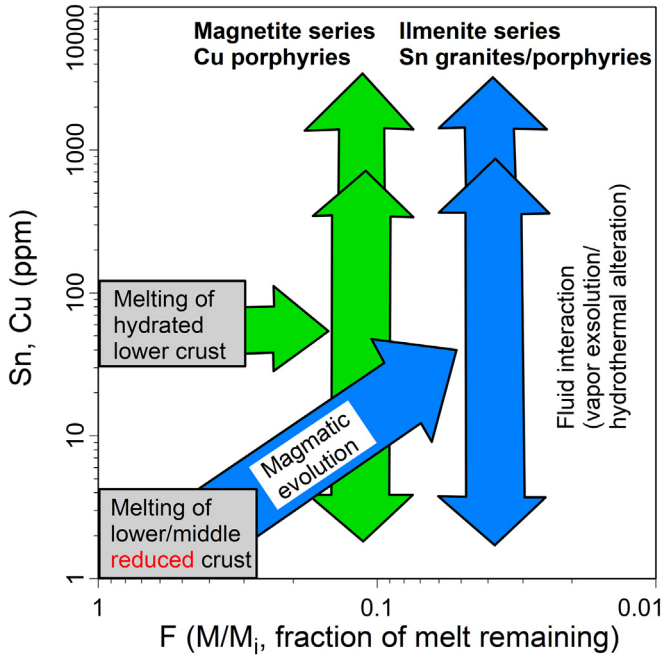

Fig. 12. Metallogenic model of granite-related ore formation: magmatic tin enrichment through fractional crystallization with D_{Sn}(crystals/melt) <1, and subsequent hydrothermal redistribution of tin. Both processes are favored by an oxidation state of the system below or at the NNO buffer, i.e. relatively reduced as expressed by ilmenite-series affinity. This is opposite to molybdenum porphyries which are also highly fractionated, but evolved under oxidizing conditions (magnetite series). Copper porphyries are less evolved, but also oxidized. The source for all porphyry/granite systems is from a mixture of mantle wedge/lower crust and middle crust, but with variable proportions within these transcrustal melt systems. Tin-rich systems have commonly most crustal input which can also provide the reducing environment needed for magmatic enrichment and hydrothermal tin redistribution. Mantle is the essential heat source.

A continuum may be expected in between the more static fluid storage in intergranular spaces and explosive fluid-melt phenomena, likely controlled by pressure, i.e. depth of emplacement (Linnen, 1998). The mobilization of the magmatically developed tin potential in a highly fractionated granite phase is possible both in the earliest stage of magmatic fluid release as well as during later invasion of the cooling intrusive system by meteoric water (or deeper magmatic water from below the solidification front). Initially, there will be a separation of both fluid systems, due to the low permeability of a melt. Fracturing during the sub-solidus evolution will lead to superposition and mixing of both fluid systems.

The hydrothermal mobility of tin is physically controlled by the nature and extent of permeability and available fluid volumina during the subsolidus cooling history of a tin granite. Both factors are favored in high-level environments. The chemical parameters pH, fO_2 and chloride activity control the tin carrying capability of a solution. Fluid-buffered low-pH conditions in hydrothermally altered rock portions (feldspar unstable) can sustain high tin contents in hydrothermal solutions even at 200°C (Heinrich, 1990).

Size and primary tin content of a granite system define the maximum quantity of extractable metal. The greatest hydrothermal tin enrichments in individual ore systems are on the order of 10^6 t Sn (ore deposit plus primary dispersion halo; e.g. Llallagua/Bolivia, Altenberg/Germany, Gejiu/South China). Tin granite subintrusions reach average primary tin levels of around 30 ppm. The hydrothermal depletion of a tin-enriched magmatic system must therefore comprise a large rock volume of up to 40 km^3, when an extraction rate of one third (10 ppm Sn) is assumed. The whole magmatic fractionation system must be at

least ten times larger in order to produce a highly fractionated tin granite subintrusion. The limiting assumption of Rayleigh fractionation with ideal $D_{Sn} = 0$ gives a minimum size of the total magmatic system of 400 km^3. More realistic conditions of a less perfect fractionation mechanism require a total melt volume on the order of 1000–2000 km^3. This is the size of magma chambers known to be associated with some caldera eruptions (Hildreth, 1981). The granite batholiths underlying the Erzgebirge and Cornwall tin provinces are about 50 times larger.

The process of hydrothermal tin extraction results in open-system distortions of primary magmatic tin distribution patterns (scatter distributions with tin deficiencies). Often, however, hydrothermal tin depletion cannot be identified clearly, which suggests relatively small extraction rates not distinguishable from the internal scatter in (pseudo)-magmatic tin enrichment trends.

A metallogenic model from a geochemical point of view is condensed in Fig. 12. This model has two basic features: 1. Magmatic tin enrichment trend: fractional crystallization of granitic melt with a bulk tin distribution coefficient D_{Sn}(crystals/melt) <1. This condition is realized in ilmenite-series granitic rocks of any origin (S-, I-, A-type) but with an oxygen fugacity below the NNO oxygen buffer, which in turn is also a precondition for effective hydrothermal depletion of magmatically tin-enriched rock volumes.

2. Hydrothermal tin redistribution pattern: magmatic fluid release during solidification of the highly fractionated tin granite system combined with interaction of the solidified granite with saline hydrothermal fluids of any origin. Loading of the hydrothermal system with magmatically enriched tin, and cassiterite deposition according to local physicochemical gradients (cooling and mixing with meteoric fluids).

Tin granites are mostly, but not exclusively, peraluminous S-type magmas typically generated in the mid- to lower-crust of back-arc regions through the partial melting of dominantly metasedimentary source rocks. These source rocks control the reduced nature of the melts. This situation is different to volcanic arcs with their more juvenile mantle signature and the link between a subducting slab leading to oxidized intermediate magmas and Cu—Au mineralization (Burnham and Ohmoto, 1980). Tin granites are commonly sourced from isotopically more evolved protoliths with less mantle input, as seen from their Sr–Nd isotope signatures, and their often elevated $\delta^{18}O$ and low ε_{Hf} of zircon (compilations in Lehmann, 1990, and Mao et al., 2019). This is different from copper porphyry systems which have the signature of hydrated mantle/lower crust (hornblende suppresses plagioclase fractionation and imprints high Sr/Y and the typical spoon-shape of the REE pattern with Tb–Tm depletion; Rohrlach and Loucks, 2005), while most tin granites have trace-element patterns compatible with normal (less water) biotite-feldspar fractionation.

The Cu–Sn polarity in the metallogeny of active continental margins is probably best seen in the textbook example of the Central Andes with the giant 30–40 Ma copper porphyries in northern Chile and the equally giant 25–10 Ma tin porphyries/granites in southernmost Peru and Bolivia (Lehmann et al., 2000a; Sillitoe et al., 1975), both N-S trending belts displaced by about 300 km and separated in time by 10–20 Ma. However, a similar polarity is also observed for the Jurassic tin granites of the Nanling Range in China and the Jurassic coastal copper belt (Mao et al., 2019), or the various Mesozoic granite belts of SE Asia (Myanmar to Malaysia) (Cobbing et al., 1986; Gardiner et al., 2016; Mao et al., 2020; Yang et al., 2020), which are, however, tectonically more complicated due to large-scale Himalayan escape (strike-slip) tectonics. Congruency of regional Cu and Sn mineralization is seen in Cornwall, which is well known for its tin deposits with a cumulative Sn production of about 2 Mt Sn, but which has also produced ≥1.3 Mt Cu (Dines, 1956). An example of a worldclass tin deposit which started out as a copper mine is San Rafael in southern Peru, with a distinct zoning pattern of distal near-surface high-grade Cu and deep high-grade tin mineralization (Mlynarczyk et al., 2003).

It appears that normal subduction is probably not sufficient for the generation of major Cu porphyry systems, as seen in the narrowly segmented distribution of Cu endowment in the Circum–Pacific region with southern Peru/northern Chile, southwestern USA and New Guinea/adjoining islands standing out (Sillitoe, 2012, 2018). A similar segmentation applies to tin, with SE Asia, South China and Bolivia/southern Peru standing out (Fig. 1). The reason for the regionally and temporally segmented metal endowment in Cu could be periods of flat slab subduction which hydrate and "fertilize" (with respect to Cu) the lower continental crust due to no or little coeval magmatism. The undiluted metal inventory then would be available for the small melt fractions produced during flat-slab subduction, for instance in transtensional strike-slip zones in the general compressive regime. (Kay and Mpodozis, 2001; Lehmann et al., 2000b) Such a model could also apply to the 5–10 Ma Cu porphyry segments of central Chile/NW Argentina and Peru, where present-day flat slab subduction of the Nazca ridge to the north and the Juan Fernandez ridge to the south has shut down major volcanism in these two arc segments (Hampel, 2002; James and Sacks, 1999; Skewes and Stern, 1995). The transition from the flat-slab compressive regime with thickening of the continental crust to an extensive regime with steepening of the subduction zone, possibly even slab rollback or delamination of lower continental crust, would then allow large-scale crustal melting by mantle upwelling in the back arc and development of locally highly evolved melt portions. Given a chemically reducing crustal lithology, such as the thick mid-upper crustal Paleozoic black shale sequence in Bolivia, these melt portions could be the source of tin mineralization. Molybdenum mineralization would derive from similarly fractionated but oxic melt portions where the chemically reducing country rocks are missing. This situation would apply to the 44–17 Ma molybdenum belt of Colorado-New Mexico, about 400 km NE of the 50–70 Ma copper porphyry systems of the American Southwest. The solubility of tungsten in melt and aqueous fluids is much less redox depedent, and this element can be associated to all evolved granite systems.

The accessory mineral zircon mirrors the bulk rock composition and carries not only valuable age information, but also information on melt source, degree of melt evolution, redox state and even hydrothermal overprint. These parameters can be constrained by in-situ LA-ICPMS analysis, and zircon geochemistry may well become an interesting exploration tool for magmatic-hydrothermal ore deposits, in particular the copper-gold to tin-tungsten spectrum. The REE patterns of zircon record the increasingly negative Eu anomaly (Eu/Eu*) with feldspar fractionation (Gardiner et al., 2017), and oxidation state correlates positively with the Ce anomaly (Ce^{4+}/Ce^{3+}; Ballard et al., 2002). It remains to be tested how much information may be gained from magmatic-hydrothermal zircon rims which may carry direct information with respect to the metal content of the vapor phase during the magmatic-hydrothermal transition.

Declaration of Competing Interest

None.

Acknowledgements

This paper developed from an invited keynote presentation at the 9th Hutton Symposium in Nanjing in October 2019. Critical comments by Guest editor Xiaolei Wang and referees Robert Linnen, Reimar Seltmann and an anonymous expert helped to improve the manuscript. Technical support by Fred Türck is acknowledged.

Declaration of interests

The authors declare that they have no known competing financial interests or personal relationships that could have appeared to influence the work reported in this paper.

References

USGS, 2020. Mineral commodity summaries 2020. U.S. Geological Survey, p. 200.

Antipin, V.S., Kovalenko, V.I., Kuznetsova, A.I., Persikova, L.A., 1981. Distribution coefficients for tin and tungsten in ore-bearing acid igneous rocks. Geochemistry International 18 (1), 92–106.

Ballard, J.R., Palin, J.M., Campbell, I.A., 2002. Relative oxidation states of magmas inferred from Ce(IV)/Ce(III) in zircon: application to porphyry copper deposits of northern Chile. Contrib. Mineral. Petrol. 144, 347–364.

Barsukov, V.L., 1957. The geochemistry of tin. Geochemistry 1, 41–52.

De Beaumont, E., 1847. Note sur les émanations volcaniques et métallifères. Bulletin Société Géologique France. 2ième Série 4, 1249–1334.

Bhalla P,, Holtz, F., Linnen, R.L., Behrens, H., 2005. Solubility of cassiterite in evolved granitic melts: effect of T, fO_2, and additional volatiles. Lithos 80, 387–400.

Bodnar, R.J., Lecumberri-Sanchez, P., Moncada, D., Steele-MacInnis, M., 2014. Fluid inclusions in hydrothermal ore deposits. In: Holland, H.D., Turekian, K.K. (Eds.), Treatise on Geochemistry, 2nd ed 13, pp. 119–142.

Breiter, K., 2012. Nearly contemporaneous evolution of the A- and S-type fractionated granites in the Krušné hory/Erzgebirge Mts., Central Europe. Lithos 151, 105–121.

Brügmann, G., Berger, D., Pernicka, E., 2017. Determination of the tin stable isotopic composition in tin-bearing metals and minerals by MC-ICP-MS. Geostand. Geoanal. Res. 41, 437–448.

Burnham, C.W., 1979. Magmas and hydrothermal fluids. In: Barnes, H.L. (Ed.), Geochemistry of Hydrothermal Ore Deposits, 2nd edn Wiley, New York, pp. 71–136.

Burnham, C.W., Ohmoto, H., 1980. Late-stage processes of felsic magmatism. Mining Geology, Special Issue 8, 1–11.

Cashman, K.V., Sparks, R.S.J., Blundy, J.D., 2017. Vertically extensive and unstable magmatic systems: a unified view of igneous processes. Science 355, eaag 3005.

Černý, P., 1991. Rare-element granitic pegmatites, part I: Anatomy and internal evolution of pegmatite deposits. Geoscience Canada 18 (2), 49–67.

Černý, P., Blevin, P.L., Cuney, M., London, D., 2005. Granite-related ore deposits. Economic Geology 100th Anniversary 337–370.

Che, X.D., Linnen, R.L., Wang, R.C., Aseri, A., Thibault, Y., 2013. Tungsten solubility in evolved granitic melts: an evaluation of magmatic wolframite. Geochimica et Cosmochimca Acta 106, 84–98.

Cobbing, E.J., Mallick, D.I.J., Pitfield, P.E.J., Teoh, L.H., 1986. The granites of the Southeast Asian tin belt. Journal of the Geological Society of London 143, 537–550.

Cotta, B. von, 1859. Die Lehre von den Erzlagerstätten. Erster Theil. 2. Auflage. Engelhardt, Freiberg, p. 252.

Daubrée, A., 1841. Mémoire sur le gisement, la constitution et l'origine des amas de minerai d'étain. Annales des Mines, 3ième Série 20, 65-112.

DeCelles, P.G., Ducea, M.N., Kapp, P., Zandt, G., 2009. Cyclicity in Cordilleran orogenic systems. Nat. Geosci. 2, 251–257.

Dietrich, A., Lehmann, B., Wallianos, A., 2000. Bulk rock and melt inclusion geochemistry of Bolivian tin porphyry systems. Econ. Geol. 95, 313–326.

Dines, H. G., 1956. The Metalliferous Mining Region of South-West England, 1 and 2. London: HMSO. 526 and 300 p.

Duc-Tin, Q., Audétat, A., Keppler, H., 2007. Solubility of tin in (Cl, F)-bearing aqueous fluids at 700°C, 140 MPa: a LA-ICP-MS study on synthetic fluid inclusions. Geochim. Cosmochim. Acta 71, 3323–3335.

Elsner, H., 2014. Zinn - Angebot und Nachfrage bis 2020. Deutsche Rohstoffagentur. DERA Rohstoffinformationen 20, 1–255.

Ericksen, G,E., Luedke, R.G., Smith, R.L., Koeppen, R.P., Urquidi, B.F., 1990. Peraluminous igneous rocks of the Bolivian tin belt. Geology 13, 3–8.

Eugster, H.P., 1986. Minerals in hot water. Am. Mineral. 71, 655–673.

Farges, F., Linnen, R.L., Broen Jr., G.E., 2006. Redox and speciation of tin in hydrous silicate glasses: a comparison with Nb, Ta, Mo and W. Can. Mineral. 44, 795–810.

Gardiner, N.J., Robb, L.J., Morley, C.K., Searle, M.P., Cawood, P.A., Whitehouse, M.J., Kirkland, C.L., Roberts, N.M.W., Myint, T.A., 2016. The tectonic and metallogenic framework of Myanmar: a Tethyan mineral system. Ore Geol. Rev. 79, 26–45.

Gardiner, N.J., Hawkesworth, C.J., Robb, L.J., Whitehouse, M.J., Roberts, N.M.W., Kirkland, C. L., Evans, N.J., 2017. Contrasting granite metallogeny through the zircon record: a case study from Myanmar. Sci. Rep. 7, 748.

Girei, M.B., Li, H., Algeo, T.J., Bute, S.I., 2019. Petrogenesis of A-type granites associated with Sn–Nb–Zn mineralization in Ririwai complex, north-Central Nigeria: Constraints from whole-rock Sm–Nd and zircon Lu–Hf isotope systematics. Lithos 340-341, 49–90.

Goethe, J.W., 1814. Zinnformation. Johann Wolfgang Goethe, Schriften zur Geologie, Mineralogie und Meteorologie. dtv-Gesamtausgabe. 38, pp. 65–67.

Grant, J.N., Halls, C., Avila, W., Avila, G., 1977. Igneous geology and the evolution of hydrothermal systems in some sub-volcanic tin deposits of Bolivia. Geological Society of London, Special Publication 7, 117–126.

Hampel, A., 2002. The migration history of the Nazca Ridge along the Peruvian active margin: a re-evaluation. Earth Planet. Sci. Lett. 203, 665679.

Haschke, M.R., Scheuber, E., Günther, A., Reutter, K.-J., 2002. Evolutionary cycles during the Andean orogeny: repeated slab breakoff and flat subduction? Terra Nova 14, 49–55.

Heinrich, C.A., 1990. The chemistry of hydrothermal tin (−tungsten) ore deposition. Econ. Geol. 85, 457–481.

Hildreth, W., 1981. Gradients in silicic magma chambers: implications for lithospheric magmatism. J. Geophys. Res. 86, 10153–10192.

Holland, H.D., 1972. Granites, solutions, and base metal deposits. Econ. Geol. 67, 281–301.

Humboldt, A. von, 1823. Essai géognostique sur le gisement des roches dans les deux hémisphères. Levrault, Strasbourg, p. 364.

Ingham, F.T., Bradford, E.F., 1960. The geology and mineral resources of the Kinta Valley, Perak. Malaya Geological Survey District Memoir 9, 1–347.

Ishihara, S., 1977. The magnetite-series and ilmenite-series granitic rocks. Mining Geology 27, 293–305.

Ishihara, S., 1981. The granitoid series and mineralization. Economic Geology 75th Anniversary Volume, 458–484.

Jackson, N.J., 1979. Geology of the Cornubian tin field: a review. Bulletin of the Geological Society of Malaysia 11, 209–237.

James, D., Sacks, I.S., 1999. Cenozoic formation of the Central Andes:a geophysical perspective. Economic Geology Special Publiction 7, l–59.

Kay, S.M., Mpodozis, C., 2001. Central Andean ore deposits linked to evolving shallow subduction systems and thickening crust. GSA Today 11, 4–9.

Kelly, W.C., Turneaure, F.S., 1970. Mineralogy, paragenesis and geothermometry of the tin and tungsten deposits of the Eastern Andes, Bolivia. Econ. Geol. 65, 609–680.

Keppler, H., Wyllie, P.J., 1991. Partitioning of Cu, Sn, Mo, W, U, and Th between melt and aqueous fluid in the systems haplogranite-H_2O-HCl and haplogranite-H_2O-HF. Contrib. Mineral. Petrol. 109, 139–150.

Kovalenko, V.I., Ryzhenko, B.N., Barsukov, V.L., Klintsova, A.P., Velyukhanova, T.K., Vlynets, M.P., Kitayeva, L.P., 1986. The solubility of cassiterite in HCl and HCl + NaCl (KCl) solutions at 500°C and 1000 atm under fixed redox conditions. Geochemistry International 23 (7), 1–16.

Kovalenko, V.I., Ryabchikov, I.D., Antipin, V.S., 1988. Temperature dependence of the distribution coefficients for Sn, W, Pb, and Zn in magmatic systems. Geochemistry International 25 (1), 1–10.

Lehmann, B., 1982. Metallogeny of tin: magmatic differentiation versus geochemical heritage. Econ. Geol. 77, 50–59.

Lehmann, B., 1990. Metallogeny of Tin. Springer, Berlin, p. 211.

Lehmann, B., Mahawat, C., 1989. Metallogeny of tin in Central Thailand: a genetic concept. Geology 17, 426–429.

Lehmann, B., Ishihara, S., Michel, H., Miller, J., Rapela, C., Sanchez, A., Tistl, M., Winkelmann, L., 1990. The Bolivian tin province and regional tin distribution in the Central Andes: a reassessment. Econ. Geol. 85, 1044–1058.

Lehmann, B., Dietrich, A., Wallianos, A., 2000a. From rocks to ore. International Journal of Earth Sciences 89, 284–294.

Lehmann, B., Dietrich, A., Heinhorst, J., Métrich, N., Mosbah, M., Palacios, C., Schneider, H.-J., Wallianos, A., Webster, J., Winkelmann, L., 2000b. Boron in the Bolivian tin belt. Miner. Deposita 35, 223–232.

Lehmann, B., Halder, S., Ruzindana Munana, J., de la Paix Ngizimana, J., Biryabarema, M., 2014. The geochemical signature of rare-metal pegmatites in Central Africa: Magmatic rocks in the Gatumba tin-tantalum mining district, Rwanda. J. Geochem. Explor. 144, 528–538.

Lehmann, B., Zoheir, B.A., Neymark, L.A., Zeh, A., Emam, A., Radwan, A.M., Zhang, R.-Q., Moscati, R.J., 2020. Monazite and cassiterite U Pb dating of the Abu Dabbab rare-metal granite, Egypt: late Cryogenian metalliferous granite magmatism in the Arabian-Nubian Shield. Gondw. Res. 84, 71–80.

Linnen, R.L., 1998. Depth of emplacement, fluid provenance and metallogeny in granitic terranes: a comparison of western Thailand with other tin belts. Miner. Deposita 33, 461–476.

Linnen, R.L., Pichavant, M., Holtz, F., 1996. The combined effects of fO_2 and melt composition on SnO_2 solubility and tin diffusivity in haplogranitic melts. Geochim. Cosmochim. Acta 60, 4965–4976.

Little, W., 1960. Inclusions in cassiterite and associated minerals. Econ. Geol. 55, 485–509.

London, D., Morgan, V.I.G.B., 2017. Experimental crystallization of the Macusani obsidian, with applications to lithium-rich granitic pegmatites. J. Petrol. 58, 1005–1030.

Mao, J.W., Cheng, Y.B., Chen, M.H., Pirajno, F., 2013. Major types and time–space distribution of Mesozoic ore deposits in South China and their geodynamic settings. Miner. Deposita 48, 267–294.

Mao, J.W., Ouyang, H.G., Song, S.W., Santosh, M., Yuan, S., Zhou, Z.H., Zheng, W., Liu, H., Liu, P., Cheng, Y., Chen, M.H., 2019. Geology and metallogeny of tungsten and tin deposits in China. Society of Economic Geologists Special Publication 22, 441–482.

Mao, W., Zhong, H., Yang, J.H., Tang, Y.W., Liu, L., Fu, Y.H., Zhang, X.C., Sein, K., Aung, S.M., Li, J., Zhang, L., 2020. Combined zircon, molybdenite, and cassiterite geochronology and cassiterite geochemistry of the Kuntabin tin-tungsten deposit in Myanmar. Econ. Geol. 115, 603–625.

Mlynarczyk, M.S.J., Sherlock, R.L., Williams-Jones, A.E., 2003. San Rafael, Peru: geology and structure of the worlds richest tin lode. Miner. Deposita 38, 555–567.

Morgan VI, G.B., London, D., Luedke, R.G., 1998. Petrochemistry of late Miocene peraluminous silicic volcanic rocks from the Morococala field, Bolivia. J. Petrol. 39, 601–632.

Moss, R., Tzimas, E., Willis, P., Arendorf, J., Tercero Espinoza, L., et al., 2013. Critical metals in the path towards the decarbonisation of the EU energy sector. Assessing rare metals as supply-chain bottlenecks in low-carbon energy technologies. Scientific and Policy report, Joint Research Centre, European Commission. Publications Office, Luxemburg, p. 242.

Müller, B., Frischknecht, R., Seward, T.M., Heinrich, C.A., Gallegos, W.C., 2001. A fluid inclusion reconnaissance study of the Huanuni tin deposit (Bolivia), using LA-ICP-MS micro-analysis. Miner. Deposita 36, 680–688.

Müller, A., Seltmann, R., Halls, C., Siebel, W., Dulski, P., Jeffries, T., Spratt, J., Kronz, A., 2006. The magmatic evolution of the Land's End pluton, Cornwall, and associated pre-enrichment of metals. Ore Geol. Rev. 28, 329–367.

Naumov, V.B., Dorofeev, V.A., Mironova, O.F., 2011. Physicochemical parameters of the formation of hydrothermal deposits: a fluid inclusion study. I. Tin and tungsten deposits. Geochemistry International 49, 1002–1021.

Nekrasov, I.Y., Epel'baum, M.B., Sobolev, V., 1980. Partitioning of tin between melt and chloride fluid in the granite–SnO–SnO_2 fluid system. Doklady Academy Sciences USSR, Earth Science Section 252, 165–168.

Neymark, L.A., Holm-Denoma, C.S., Larin, A.M., Moscati, R.J., Plotkina, Y.V., 2020. LA-ICPMS U-Pb dating reveals cassiterite inheritance in the Yazov Granite, eastern Siberia: Implications for tin mineralization. Mineralium Deposita, submitted.
Pichavant, M., 1981. An experimental study of the effect of boron on a water-saturated haplogranite at 1 kbar vapour pressure. Contrib. Mineral. Petrol. 76, 430–439.
Pichavant, M., Kontak, D.J., Briqueu, L., Herrera, J.V., Clark, A.H., 1988. The Miocene-Pliocene Macusani volcanics, SE Peru. II. Geochemistry and origin of a felsic peraluminous magma. Contributions to Mineralogy and Petrology 100, 325–338.
Pollard, P.J., Taylor, R.G., 1986. Progressive evolution of alteration and tin mineralization: controls by interstitial permeability and fracture-related tapping of magmatic fluid reservoirs in tin granites. Econ. Geol. 81, 1795–1800.
Pollard, P.J., Pichavant, M., Charoy, B., 1987. Contrasting evolution of fluorine- and boron-rich tin systems. Miner. Deposita 22, 315–321.
Pollard, P.J., Nakapadungrat, S., Taylor, R.G., 1995. The Phuket Supersuite, South Thailand: Fractionated I-type granites associated with tin-tantalum mineralization. Econ. Geol. 90, 586–602.
Raimbault, L., Cuney, M., Azencott, C., Duthou, J.-L., Joron, J.-L., 1995. Geochemical evidence for a multistage magmatic genesis of Ta-Sn-Li mineralization in the granite at Beauvoir, French Massif Central. Econ. Geol. 90, 548–576.
Richards, J., 2018. A shake-up in the porphyry world? Econ. Geol. 113, 1225–1233.
Roedder, E., 1984. Fluid inclusions. Reviews in Mineralogy 12, 1–646.
Rohrlach, B.D., Loucks, R.E., 2005. Multi-million-year cyclic ramp-up of volatiles in a lower crustal magma reservoir trapped below the Tampakan copper-gold deposit by Mio-Pliocene crustal compression in the southern Philippines. In: Porter, T.M. (Ed.), Super porphyry copper and gold deposits: a global perspective, 2nd ed. PGC Publishing, Adelaide, pp. 369–407.
Romer, R.L., Kroner, U., 2015. Sediment and weathering control on the distribution of Paleozoic magmatic tin-tungsten mineralization. Miner. Deposita 50, 327–338.
Romer, R.L., Kroner, U., 2016. Phanerozoic tin and tungsten mineralization -Tectonic controls on the distribution of enriched protoliths and heat sources for crustal melting. Gondw. Res. 31, 60–95.
Rößler, B., 1700. Speculum metallurgiae politissimum. Oder: Hell-polierter Berg-Bau-Spiegel. Johann Jacob Winckler, Dresden, p. 168.
Routhier, P., 1967. Essai critique sur les méthodes de la géologie. De l'objet à la genèse. Masson, Paris, p. 204.
Routhier, P., 1983. Where Are the Metals for the Future? The metal provinces. An essay of global metallogeny. BRGM, Orléans, p. 400.
Rudnick, R.L., Gao, S., 2003. Composition of the continental crust. Treatise in Geochemistry 3, 1–64.
Sandeman, H.A., Clark, A.H., 2003. Glass-rich, cordierite-biotite rhyodacite, Valle Ninahuisa, Puno, SE Peru: Petrological evidence for hybridization of 'Lachlan S-type' and potassic mafic magmas. J. Petrol. 44, 355–385.
Schmidt, C., 2018. Formation of hydrothermal tin deposits: Raman spectroscopic evidence for an important role of aqueous Sn(IV) species. Geochim. Cosmochim. Acta 220, 499–511.
Schneider, H.-J., Lehmann, B., 1977. Contribution to a new genetical concept on the Bolivian tin province. In: Klemm, D.D., Schneider, H.-J. (Eds.), Time- and Strata-Bound Ore Deposits. Springer, Berlin, Heidelberg, pp. 153–168.
Schuiling, R.D., 1967. Tin belts on the continents around the Atlantic Ocean. Econ. Geol. 62, 540–550.
Sillitoe, R.H., 2012. Copper provinces. In: Hedenquist, J.W., Harris, M., Camus, F. (Eds.), Geology and genesis of major copper deposits and districts of the world: a tribute to Richard H. Sillitoe. 16. Society of Economic Geologists, Special Publication, pp. 1–18.
Sillitoe, R.H., 2018. Why no porphyry copper deposits in Japan and South Korea? Resource Geology 68, 107–125.
Sillitoe, R.H., Halls, C., Grant, J.N., 1975. Porphyry tin deposits in Bolivia. Econ. Geol. 70, 913–927.
Sinclair, W.D., Gonevchuk, G.A., Korostelev, P.G., Semenyak, B.I., Rodionov, S.M., Seltmann, R., Stemprok, M., 2014. World tin and tungsten deposit database. Geological Survey of Canada, Open File 7688, 1 .zip file. doi:https://doi.org/10.4095/295581
Skewes, A., Stern, C., 1995. Genesis of the giant late Miocene to Pliocene copper deposits of Central Chile in the context of Andean magmatic and tectonic evolution. International Geology Review 37, 893–909.
Sparks, R.S.J., Huppert, H.E., Turner, F.R.S., 1984. The fluid dynamics of evolving magma chambers. Philosophical Transactions Royal Society A 310, 511–534.
Sparks, R.S.J., Annen, C., Blundy, J.D., Cashman, K.V., Rust, A.C., Jackson, M.D., 2019. Formation and dynamics of magma reservoirs. Philosophical Transactions Royal Society A 377, 20180019.
Stepanov, A., Mavrogenes, J.A., Meffre, S., Davidson, P., 2014. The key role of mica during igneous concentration of tantalum. Contrib. Mineral. Petrol. 167, 1009.
Sylvester, P.J., 1998. Post-colisional strongly peraluminous granites. Lithos 45, 29–44.
Taylor, R.G., 1979. Geology of Tin Deposits. Elsevier, Amsterdam, p. 543.
Taylor, S.R., McLennan, S.M., 1985. The Continental Crust: Its Composition and Evolution. Blackwell, Oxford, p. 312.
Tischendorf, G., 1989. Silicic magmatism and metallogenesis of the Erzgebirge (compiled by G. Tischendorf). Veröffentlichungen Zentralinstitut der Physik der Erde (Potsdam) 107, 1–316.
Vonopartis, L., Nex, P., Kinnaird, J., Robb, L., 2020. Evaluating the chnges from endogranitic magmatic to magmatic-hydrothermal mineralization: the Zaaiplaats tin granites, Bushveld Igneous complex, South Africa. Minerals 10, 379. https://doi.org/10.3390/min10040379.
Watson, E.B., 1979. Zircon saturation in felsic liquids: Experimental results and applications to trace element geochemistry. Contrib. Mineral. Petrol. 70, 407–419.
Wilson, G.A., Eugster, H., 1990. Cassiterite solubility and tin speciation in supercritical chloride solution. In: Spencer, R.J., Chou, I. Ming (Eds.), Fluid-Mineral Interactions. A Tribute to H.P. Eugster. 2. Geochemical Society, Special Publication, pp. 179–195.
Wood, S.A., Samson, I.M., 2000. The hydrothermal geochemistry of tungsten in granitoid environments: I. Relative solubilities of ferberite and scheelite as a function of T, p, pH, and m_{NaCl}. Econ. Geol. 95, 143–182.
Yang, J.-H., Zhou, M.-F., Hu, R.-Z., Zhong, H., Williams-Jones, A.E., Liu, L., Zhang, X.-C., Fu, Y.-Z., Mao, W., 2020. Granite-related tin metallogenic events and key controlling factors in Peninsular Malaysia, Southeast Asia: New insights from cassiterite U-Pb dating and zircon geochemistry. Econ. Geol. 115, 581–601.
Yao, J., Mathur, R., Powell, W., Lehmann, B., Tornos, F., Wilson, M., Ruiz, J., 2018. Sn-isotope fractionation as a record of hydrothermal redox reactions. Am. Mineral. 103, 1591–1598.
Zajacz, Z., Halter, W.E., Pettke, T., Guillong, M., 2008. Determination of fluid/melt partition coefficients by LA-ICPMS analysis of co-existing fluid and silicate melt inclusions: Controls on element partitioning. Geochim. Cosmochim. Acta 72, 2169–2197.
Zhang, R.Q, Lehmann, B., Seltmann, R., Sun, W.D., Li, C.Y., 2017. Cassiterite U-Pb geochronology constrains magmatic-hydrothermal evolution in complex evolved granite systems: the classic Erzgebirge tin province (Saxony and Bohemia). Geology 46, 1095–1098.
Zhang, S., Zhang, R.Q., Lu, J.J., Ma, D.S., Ding, T., Gao, S.Y., Zhang, Q., 2019. Neoproterozoic tin mineralization in South China: geology and cassiterite U-Pb age of the Baotan tin deposit in northern Guangxi. Miner. Deposita 54, 1125–1142.
Zoheir, B., Lehmann, B., Emam, A., Radwan, A., Zhang, R., Bain, W.M., Steele-MacInnis, M., Nolte, N., 2020. Extreme fractionation and magmatic-hydrothermal transition in the formation of the Abu Dabbab rare-metal granite, Eastern Desert, Egypt. Lithos 352-353, 105329.